Adsorption cooling system employing novel MIL-101(Cr)/$CaCl_2$ composites: Numerical study

Eman Elsayed[a,b,*], Raya AL-Dadah[a], Saad Mahmoud[a], Paul Anderson[b], Ahmed Elsayed[c]

[a] Department of Mechanical Engineering, University of Birmingham, Birmingham, B15 2TT, United Kingdom.

[b] School of Chemistry, University of Birmingham, Birmingham, B15 2TT, United Kingdom.

[c] Department of Mechanical Engineering, Kingston University, SW15 3DW, United Kingdom.

* Corresponding author. E-mail: EXH496@alumni.bham.ac.uk; eng.eman.m.elsayed@gmail.com

Abstract

Due to the significant increase in the global temperature, the demand for cooling is dramatically rising. Most of this demand is met by conventional systems driven by electricity generated using fossil fuels contributing in the global warming phenomenon. The adsorption system is a sustainable system being driven by waste or low-grade heat sources such as solar energy. MIL-101(Cr) is a metal-organic framework (MOF) material with exceptional properties and high-water uptake. Nevertheless, it is not suitable for adsorption cooling application as the high capacity is taking place only at high relative pressure range (>0.5). The water adsorption characteristics of MIL-101(Cr) were significantly enhanced through incorporating the material with calcium chloride. Results showed that at desorption temperature of 90°C and a chilled water inlet temperature of 10°C, the SCP increased from 168 for the neat MIL-101(Cr) to 248 and 388 W kg^{-1} for Comp_1:5 and Comp_1:8 $CaCl_2$ composites, respectively outperforming the long dominating silica gel.

Keywords: Metal-organic framework, MIL-101(Cr), MIL-101(Cr)/$CaCl_2$ composites, adsorption cooling, numerical modelling.

Nomenclature

Symbols	***Description***	***Unit***
A	Adsorption potential	J mol^{-1}
COP	Coefficient of performance	
c_p	Specific heat at constant pressure	J kg^{-1} K^{-1}
D_{so}	Pre-exponential constant of the effective vapour diffusivity	m^2 s^{-1}
D_s	Surface diffusion coefficient	m^2 s^{-1}
E_a	Activation energy	J mol^{-1}
F	constant	–
h_{fg}	Latent heat of vapourization	J $(kg\ K)^{-1}$
$K_s a_v$	Overall mass transfer coefficient	s^{-1}
K_0	LDF model empirical constant	s^{-1}
M	Mass	kg
$\dot{m}$	Mass flow rate	Kg s^{-1}
P	Pressure	kPa
P_s	Saturation pressure of adsorbate at adsorption temperature	kPa
$\frac{P}{P_S}$	Relative pressure	–
Q	Heat	J kg^{-1}
Q_{st}	Isosteric heat of adsorption	J kg^{-1}
R	Ideal gas constant	J $(mol\ K)^{-1}$
R_p	Radius of adsorbent particle	m
SA	Surface area	m^2
SCP	Specific Cooling Power	W kg^{-1}
T	Temperature	K
t	time	s
U	Heat transfer coefficient	W m^{-2} K^{-1}
x	Maximum uptake	$g_{H2O}.g_{ads}^{-1}$
x_0	uptake	$g_{H2O}.g_{ads}^{-1}$

Subscripts

a	Adsorbent material
ads	Adsorption
$chill$	Chilled

cond	Condenser
des	Desorption
evap	Evaporator
H.Ex	Heat exchanger
in	Inlet
out	Outlet
v	Vapour
w	Water

Abbreviations

DVS	Dynamic vapour sorption
EDX	Energy-dispersive X-ray spectroscopy
EU	European union
MOF	Metal-organic framework
IUPAC	International Union of Pure and Applied Chemistry
LDF	Linear driving force
MIL	Materials Institute Lavoisier
ODE	Ordinary differential equation
SWS	Selective water sorbent
TMAOH	Tetramethyl ammonium hydroxide
UMC	Unsaturated metal centers
VC	Vapour compression
XRF	X-ray fluorescence

1. Introduction

Recently, the world has witnessed a significant increase in the CO_2 emissions. This caused the average global temperature to increase at the fastest rate in the recorded history (Henley, 2015). To overcome such increase, the demand of cooling has also increased and most of this cooling demand is met by mechanical vapour compression (VC) systems which are driven by high grade electrical power sources generated using fossil fuels causing the global warming phenomenon.

The EU countries committed the temperature increase to well below 2 K above pre-industrial levels through the Paris Agreement in 2015 aiming to shift the EU by 2020 towards a low-carbon economy based on renewable energy sources and energy efficiency . To meet the previous requirement and control the average global temperature rise, cleaner and more energy efficient technologies must be used.

An effective alternative to the common VC systems is adsorption systems which have been proven to be sustainable and possessing important advantages such as being driven by waste or low-grade heat sources such as solar energy and using environmentally friendly refrigerants such as water. The system also has no moving parts except few actuating valves hence low maintenance cost is expected.

In a basic adsorption cycle (**Fig. 1**), the refrigerant is evaporated, taking its evaporation heat from the surroundings and thereby producing useful cold (when used in cooling applications). Then the vapour is adsorbed into the porous adsorbent material, generating the heat of adsorption. This heat is either released to the environment in the cooling case or used as useful heat in the heat pump application. In the desorption process, the porous adsorbent is regenerated (dried) by applying heat from external heat sources that can be solar energy or industrial waste heat. Finally, the desorbed refrigerant is condensed at a medium temperature level, releasing the heat of condensation, which is useful in the heat pump application or is released to the environment in cooling applications (Elsayed et al., 2017b).

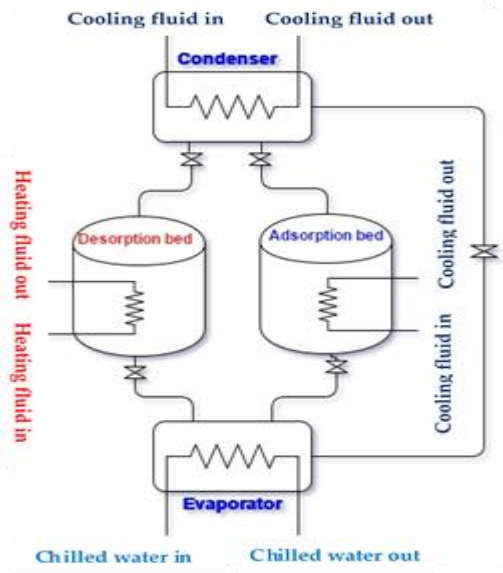

Fig. 1 Schematic diagram of the adsorption system.

For adsorption cooling, adsorbents such as silica gel, zeolites and activated carbons have been used with numerous refrigerants. Silica gel is mainly used with water giving a specific cooling power (SCP) ranging from 80 to 288 W kg^{-1} and a coefficient of performance (COP) of 0.3 (Hamamoto et al., 2005; Khan et al., 2006) while using it with methanol gave an SCP of 100 W kg^{-1} and COP of 0.3 (Mande et al., 2000). Other adsorbents such as activated carbon are mainly used with methanol or ammonia giving an SCP of 170-800 W kg^{-1} and COP of 0.2-0.5 (Critoph et al., 2010; Wu et al., 2002) while the adsorbent pair of zeolite and water can give an SCP of 135 and COP of 0.68 (Poyelle et al., 1999). Nevertheless, the above COP (an indication of the cycle efficiency) and the SCP values are considered to be lower than the ones produced from the VC system due to the limited amount of the adsorbed refrigerant circulated in the adsorption system (Qadir et al., 2016; Rezk et al., 2012). To solve such problem, new adsorbent materials with improved adsorption properties (Saha et al., 2011; Zhang and Dincer, 2017) or new adsorption bed designs (Graf et al., 2016) need to be proposed.

Metal–organic frameworks (MOFs) are porous materials that have attracted considerable research due to their ultrahigh surface area and tunable pore structures. MOFs have been investigated in adsorption heat pump application where they showed better performance compared to conventional adsorbents like silica gel and zeolite (Henninger et al., 2009; Henninger et al., 2012; Jeremias et al., 2014; Jeremias et al., 2012; Rezk et al., 2012; Rezk et al., 2013). MIL-101(Cr), is one of the most investigated MOFs due to its high

pore volume, the exceptional high surface area, high water uptake (≥ 1 g_{H2O} g_{ads}^{-1} at high relative pressure > 0.5) and high cyclic stability (Ehrenmann et al., 2011; Henninger et al., 2012; Janiak and Henninger, 2013; Khutia et al., 2013; Zhengqiu et al., 2014). The relative pressure is defined as the ratio between the equilibrium pressure and the saturation pressure of the refrigerant at a certain temperature. The water vapour adsorption capacity of MIL-101(Cr) was increased further to reach 1.58 g_{H2O} g_{ads}^{-1} by synthesizing a composite of MIL-101(Cr) and graphite oxide (Yan et al., 2015) while a composite of MIL-101(Cr) and graphene oxide showed an enhancement in the thermal conductivity and water uptake (Elsayed et al., 2017b). Nevertheless, all previously conducted studies focused on improving the equilibrium water vapour capacity of MIL-101(Cr), meaning that the entire enhancement took place at the high relative pressure (> 0.5) (**Fig. 2**). Adsorbents that can be used in adsorption cooling application should have a high vapour uptake at a relative pressure <0.4 (**Fig. 2**), hence MIL-101(Cr) and its previously synthesized composites are impractical for such application.

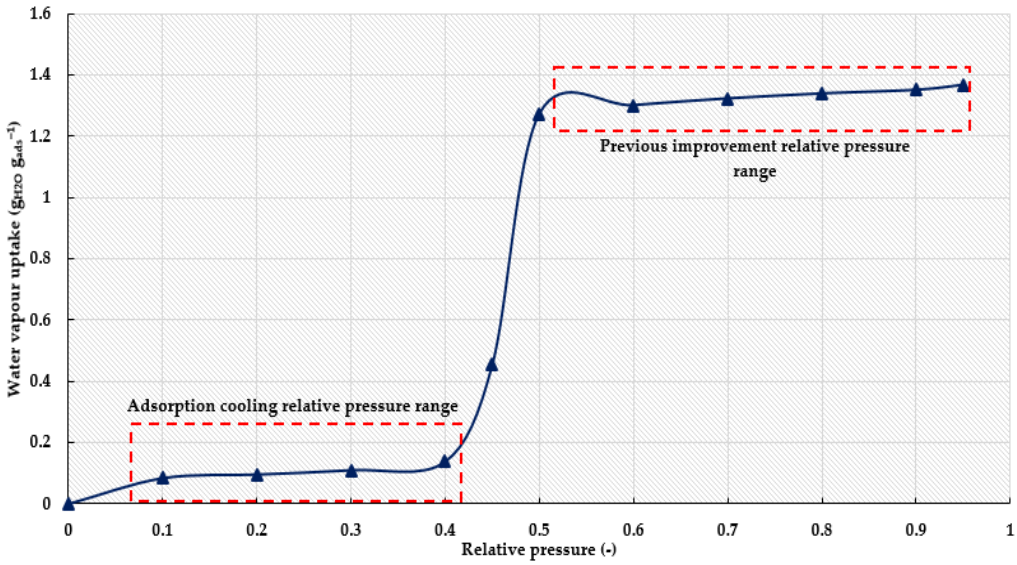

Fig. 2 Water adsorption isotherm of MIL-101(Cr) indicating the relative pressure range of the adsorption cooling application and previous enhancement in the water adsorption capacity.

In this study, the water vapour capacity of neat MIL-101(Cr) in the low relative pressure range (<0.5) was significantly improved through synthesizing novel MIL-101(Cr)/$CaCl_2$ composites. Calcium chloride is a hygroscopic salt that has a strong affinity for water. It was reported that a significant improvement was observed when the salt was incorporated with other porous material (hosting matrix) such as activated carbon, silica gel and zeolites to form composites. One of the earliest studies was conducted by (Aristov et al., 1996) discussing a composite of silica gel/$CaCl_2$ known as selective water sorbent (SWS-1L) which became later a subject of extensive studies. The enhancement in the water vapour capacity increased the COP from 0.48 to 0.7 when using a desorption temperature of 90ºC, an evaporation temperature of 5ºC, a condenser and adsorption temperatures of 40ºC (Aristov et al., 2002). Another group, (Tso and Chao, 2012), showed that the uptake was significantly improved through impregnating activated carbon with silica-gel and different concentrations of $CaCl_2$ solutions. This enhancement significantly improved the COP from 0.37 using only activated carbon to 0.7 while the SCP was increased from 65 to 387 W kg^{-1}

using the same composite at 27 °C and a water vapour pressure of 900 Pa. While a composite of activated carbon fibre felts (ACF FELT) and 30% calcium chloride had a water uptake of 1.7 $g_{H_2O}\ g_{ads}^{-1}$ which is higher than the uptake of activated carbon, silica gel and even the silica gel/$CaCl_2$ composite that had a maximum uptake of 0.5 $g_{H_2O}\ g_{ads}^{-1}$ (Wang et al., 2016). Soaking zeolite 13X in 46% $CaCl_2$ solution showed a similar improvement as a 0.4 $g_{H_2O}\ g_{ads}^{-1}$ difference in the maximum capacity was observed between 25 and 75°C at 870 Pa (Chan et al., 2012)

In the present study, incorporating MIL-101(Cr) with $CaCl_2$ salt increased the water vapour capacity from 0.1 $g_{H2O}\ g_{ads}^{-1}$ for the neat MIL-101(Cr) to 0.6 $g_{H2O}\ g_{ads}^{-1}$ for the Comp_1:8 $CaCl_2$ composite at a relative pressure of 0.4. The superior performance of the composites was assessed through developing a two-bed adsorption SIMULINK model where results showed that the SCP increased from 168 for the neat MIL-101(Cr) to 248 and 388 W kg^{-1} for Comp_1:5 and Comp_1:8 $CaCl_2$ composites, respectively. This shows that the MIL-101(Cr)/$CaCl_2$ composites outperformed the neat material at all the chilled water temperatures, highlighting the potential of using such novel adsorbent composites in adsorption cooling application.

2. Experimental work

2.1. Synthesis of MIL-101(Cr)

MIL-101(Cr) was synthesized via a hydrothermal method reported by (Yang et al., 2010). Detailed synthesis procedures can be find elsewhere (Elsayed et al., 2017b).

2.2. Synthesis of MIL-101(Cr)/$CaCl_2$ composites

Novel MIL-101(Cr)/$CaCl_2$ composites were synthesized through suspending the pre-synthesised MIL-101(Cr) powder with solutions of different $CaCl_2$ concentration with the mass ratio of one-part MIL-101(Cr) to 3, 4, 5, 6 and 8 parts of $CaCl_2$ salt. The composites were assigned the names Comp_1:3, Comp_1:4, Comp_1:5, Comp_1:6 and Comp_1:8. The $CaCl_2$ salt was dissolved in water and MIL-101(Cr) powder was added. The suspension was stirred, filtered, repeatedly washed with water to ensure that all the excess superficial $CaCl_2$ salt molecules were removed and finally the composites were left to dry in air.

2.3. Water adsorption characteristics:

The variation in water vapour uptake with the equilibrium pressure at a constant temperature (known as the adsorption isotherm) for MIL-101(Cr) and its $CaCl_2$ composites was measured using the DVS (Dynamic Vapour Sorption). As highlighted earlier, MIL-101(Cr) is only suitable for applications working at high relative pressure or high evaporation temperatures. This means that the material is not suitable for adsorption cooling applications due to its limited uptake in the low relative pressure range. This problem was addressed through synthesizing MIL-101(Cr)/$CaCl_2$ composites. The composites were divided into low $CaCl_2$ concentration composites and high $CaCl_2$ concentration composites. **Fig. 3a** shows the water adsorption isotherms of the neat material and the low $CaCl_2$ concentration composites (Comp_1:3,

Comp_1:4 and Comp_1:5) that also exhibited type IV isotherms. Nevertheless, it can be noticed that introducing the $CaCl_2$ significantly enhanced the water vapour uptake especially for Comp_1:5 $CaCl_2$ composite. This is attributed to the hygroscopic nature of $CaCl_2$ and its high affinity for water. At a relative pressure higher than 0.5, it can be noticed that all the composites have lower water vapour capacity. This can be attributed to the pores being partially filled with the salt and hence the accessible pores and surface area for the water molecules decreased causing the water vapour uptake to decrease. At higher relative pressure (≥0.5), the pores are almost filled exhibiting a stable uptake. **Fig. 3b** shows the water adsorption isotherm of the high $CaCl_2$ concentration composites (Comp_1:6 and Comp_1:8). It can be noticed, that Comp_1:6 maintained the type IV isotherm, while increasing the concentration of the $CaCl_2$ further changed the isotherm to type II in Comp_1:8 composite. The high uptake at the high relative pressure is due to the formation of the multilayer of multi-molecules where the adsorbed layers are bulk liquid (Rouquerol et al., 2013).

The enhancement in the water vapour capacity in the MIL-101(Cr)/$CaCl_2$ composites is due to either; (1) an ion exchange mechanism where the ions of the salt replace the ions of the framework. A similar mechanism was observed when $CaCl_2$ was incorporated in zeolite 13X (Chan et al., 2012); or (2) the deposition (accommodation) of the salt inside the pores of MIL-101(Cr), such mechanism was reported when $CaCl_2$ was incorporated in silica gel to produce SWS-1L (Aristov et al., 2002; Aristov et al., 1996). At the low $CaCl_2$ concentrations, the first scenario is expected to take place. In this case, a decrease in the accessible surface area is expected due to the different ion size as the size of the chloride ion is in the range of 1.81 Å while the size of the hydroxide ion is only 0.958 Å, hence a decrease in the equilibrium uptake compared to neat MIL-101(Cr) is expected to take place as shown in **Fig. 3a**. As the $CaCl_2$ concentration gradually increases, scenario two is expected to take place where the $CaCl_2$ is accommodated in the pores of the material. In this case, the pores are being partially filled with the salt and hence the accessible pores and surface area for the water molecules decreased causing the equilibrium water vapour uptake to decrease. These mechanisms were supported through performing the elemental analysis of the different $CaCl_2$ composites using both Energy-dispersive X-ray spectroscopy (EDX) and X-ray fluorescence (XRF) techniques. **Table 1a** shows the elemental analysis of the MIL-101(Cr) composites expressed as a mass ratio between the main elements in the composite (Cr, Cl and Ca) measured using both EDX and XRF techniques. This approach is well known and has been used previously in (Férey et al., 2005) and (Zhao et al., 2015). It can be noticed that with low concentration of $CaCl_2$ salt (Comp_1:3), there were no traces of Ca^{2+} but as the salt concentration increased, the concentration of the calcium ion increased (Comp_1:4 to Comp_1:8). The molar percentage of Ca^{2+} and Cl^- was then calculated as shown in **Table 1b** giving the same conclusion that in case of low $CaCl_2$ composites, only Cl^- is present proving the ion exchange mechanism while in case of high $CaCl_2$ composites, the Ca^{2+} concentration increases forming $CaCl_2$ which is accommodated in the pores and hence it is appearing in the elemental analysis.

It can be concluded from **Fig. 3a** and **Fig. 3b** that introducing the $CaCl_2$ significantly enhanced the water adsorption characteristics at the low relative pressure range. Detailed information on the water adsorption isotherm mechanism are further discussed elsewhere (Elsayed et al., 2019)

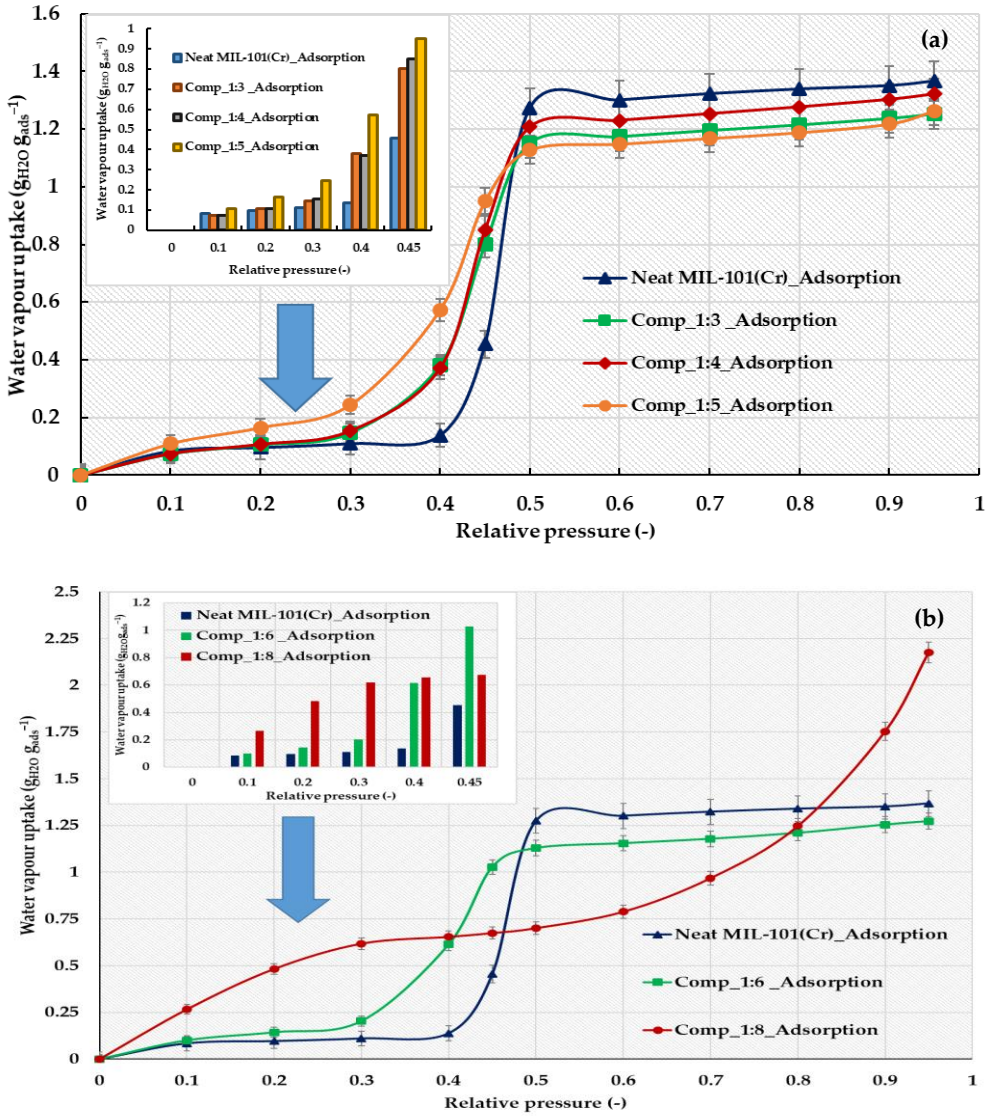

Fig. 3 a. Water adsorption isotherms of neat MIL-101(Cr) and $CaCl_2$ composites: Comp_1:3, Comp_1:4 and Comp_1:5 and b. Water adsorption isotherms of neat MIL-101(Cr) and $CaCl_2$ composites: Comp_1:6 and Comp_1:8 at 25°C.

Table 1a Elemental analysis of $CaCl_2$ composites using EDX and XRF as a mass ratio:

	EDX		XRF	
Material	Cr/Cl	Ca/Cl	Cr/Cl	Ca/Cl
Comp_1:3	7.18	0	7.1	0.01
Comp_1:4	5.42	0.04	5.2	0.05
Comp_1:5	3.5	0.20	3.56	0.21
Comp_1:6	2.5	0.25	2.9	0.29
Comp_1:8	0.54	0.48	0.7	0.5

Table 1b Elemental analysis of Ca and Cl in the $CaCl_2$ composites as molar percentage:

	Ca (% mol)	Cl (% mol)
Comp_1:3	0	0.78
Comp_1:4	0.06	1.35
Comp_1:5	1.41	1.59
Comp_1:6	1.53	2.7
Comp_1:8	1.65	3.79

2.3.1. Adsorption isotherms and kinetics models:

As Comp_1:5 and Comp_1:8 had the highest water vapour uptake (**Fig. 3a** and **Fig. 3b**), they will be furtherly investigated.

The isotherms of the composites were developed in terms of the adsorption potential (A) to show the effect of temperature on the adsorption capacity based on the work of *Polanyi* (Goldmann and Polanyi, 1928; Polanyi, 1963) (**Eq. 1**). The proposed approach was employed to fit the measured isotherms in different adsorption potential 'A' regions. Such approach has been previously employed by (Schicktanz and Núñez, 2009) and (Tokarev et al., 2005)

$$A = -RT\ln(\frac{P}{P_s}) \quad \textbf{(1)}$$

The developed equations were used to predict the water uptake at a wide range of operating conditions.

Comp_1:5 composite adsorption isotherms were measured at 15°C, 25°C and 35°C and fitted using **Eq. 2** to **Eq. 4**.

$$x = 0.64\exp(-3E - 4A) \quad A > 3700 \quad \textbf{(2)}$$

$$x = 16.6 - 1.8E - 2A + 7.8E - 6A^2 - 1.5E - 9A^3 + 1E - 13A^4 \quad 1840 < A \leq 3700 \quad \textbf{(3)}$$

$$x = 1.34 - 6.5E - 4A + 7.5E - 7A^2 - 2.7E - 10A^3 \quad A \leq 1840 \quad \textbf{(4)}$$

Fig. 4a shows the good agreement between the proposed isotherm model and the experimental data in case of Comp_1:5 composite.

Comp_1:8 composite adsorption isotherms were measured at 15°C, 25°C and 35°C and fitted using **Eq. 5** to **Eq. 7**.

$$x = 1.65\exp(-3.2E - 4A) \quad A > 2700 \quad \textbf{(5)}$$

$$x = 1.1 - 3.3E - 4A + 5.6E - 8A^2 \quad 1200 \leq A \leq 2700 \quad \textbf{(6)}$$

$$x = 2.45 - 2.8E - 3A + 1.2E - 6A^2 \quad 1200 > A \quad \textbf{(7)}$$

Fig. 4b shows the good agreement between the proposed isotherm model and the experimental data in case of Comp_1:8 composite.

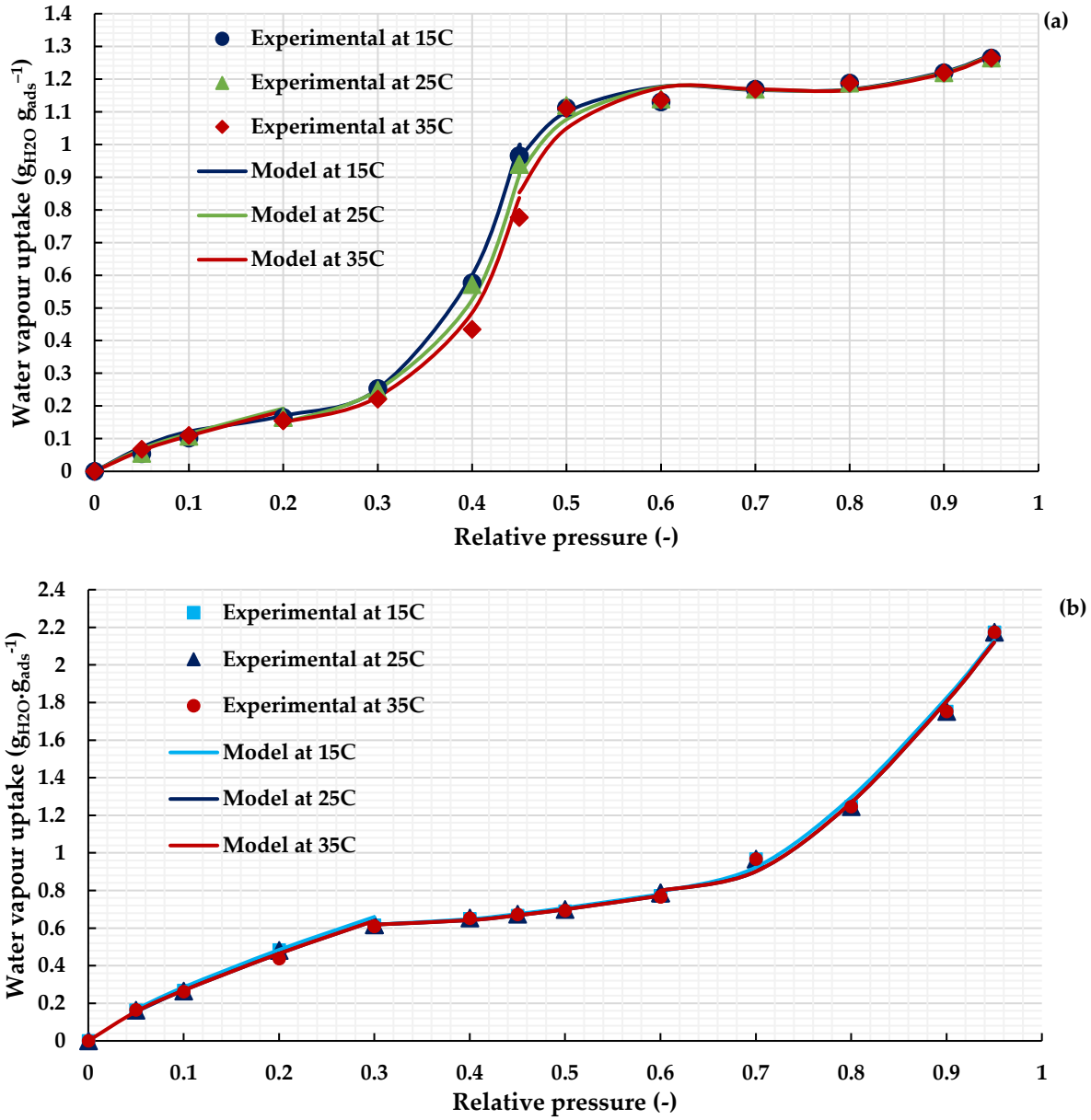

Fig. 4 a. Proposed isotherm model fitting of water adsorption on Comp_1:5 and b. Proposed isotherm model fitting of water adsorption on Comp_1:8 at different adsorption temperatures.

The performance stability of the MIL-101(Cr)/$CaCl_2$ composites was investigated through subjecting the materials to ten successive adsorption/desorption cycles. As the main improvement in the water uptake took place below a relative pressure of 0.5, the cyclic analysis was investigated in the relative pressure range of 0-0.45. As shown in **Fig. 5,** the composites had a steady performance over the tested cycles and the high uptake was not affected by the successive adsorption/desorption processes.

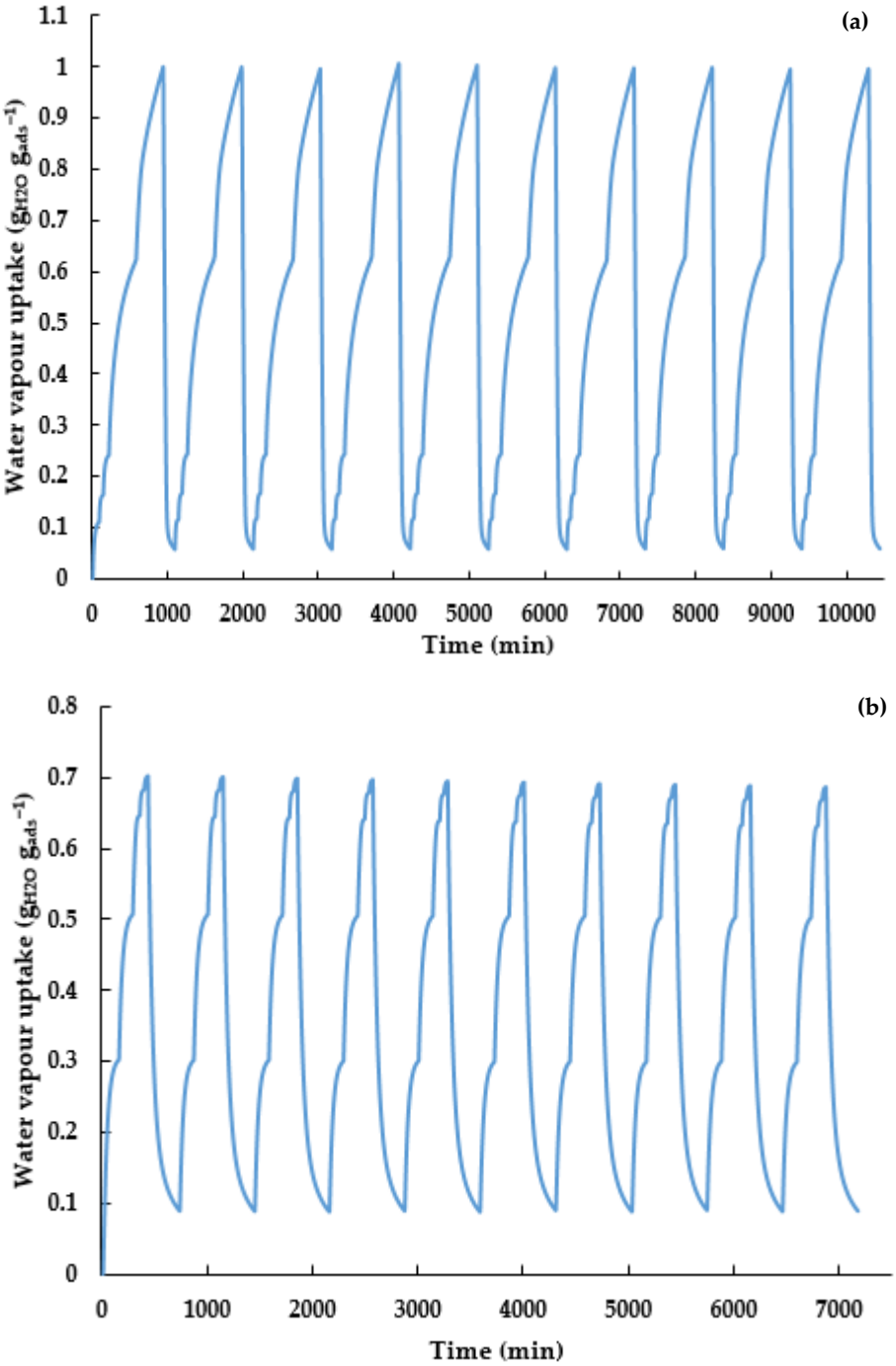

Fig. 5 Cyclic analysis (10 adsorption/desorption cycles) of $CaCl_2$ composites: a. Comp_1:5 and b. Comp_1:8 at 25°C.

The rate of adsorption or the adsorption kinetics is another crucial parameter determining the residence time required for the completion of the adsorption cycle and depending on the interaction between the adsorbent and the adsorbate. The linear driving force (LDF) was chosen to describe the adsorption rate as it has been widely known for being simple, analytically and physically consistent (Lefebvre et al., 2016). This model assumes that the adsorption rate of a particle is direct proportional to the difference between the inside and outside adsorbate concentrations of adsorbent particles (Wang et al., 2016) and that adsorption rate on the surface is much faster than the rate of inner diffusion so the kinetics on the surface are not considered rate-limiting (Bimbo et al., 2016; Narayanan et al., 2014; Niazmand et al., 2013). Linear

driving force model has been one of the most used kinetics models as it is applicable to a wide range of adsorbents for the previously mentioned reasons. **Eq. 8** to **Eq. 11** represent the LDF model.

$$\frac{dx}{dt} = K_s a_v (x - x_0) \quad \textbf{(8)}$$

$$\frac{dx}{dt} = K_0 . \exp\left[-\frac{E_a}{R.T} \right] (x - x_0) \quad \textbf{(9)}$$

$$K_0 = \frac{F D_{S0}}{R_p^2} \quad \textbf{(10)}$$

$$D_s = D_{S0} \exp\left[-\frac{E_a}{R.T} \right] \quad \textbf{(11)}$$

Where F is a constant depending on the shape of the adsorbent particles and is assumed 15 for spherical particles. The activation energy (E_a) which is defined as the minimum amount of energy that adsorbate needs to be overcome to interact with the adsorbent surface (Saha and Chowdhury, 2011) and the empirical constant (K_0) were evaluated through calculating the fractional uptake at each adsorption step, a linear plot of ln(1-fractional uptake) versus time allows the evaluation of the diffusional time constant at each step. An average value was then calculated for each temperature, the Arrhenius equation is then used to investigate the effect of temperature on the diffusion time constant and find the values of E_a and K_0. The constants were calculated according to previously published procedures (Ali et al., 2018; El-Sharkawy et al., 2015; El-Sharkawy et al., 2014; Sultan et al., 2016). The data giving the change in the mass with time at different relative pressure steps generated from the dynamic vapour sorption (DVS) test facility was used to develop the kinetics models. **Table 2** gives the values of parameters E_a and K_0 which were obtained through fitting the generated data following the methodology in (Ali et al., 2018; El-Sharkawy et al., 2015; El-Sharkawy et al., 2014; Sultan et al., 2016). **Fig. 6a** and **b** highlight the validity of the LDF model in fitting the experimental data of the materials under investigation.

Table 2 values of parameters E_a and K_0

Material	Relative pressure range	E_a (J mol^{-1})	K_0 (s^{-1})
Comp_1:5	<0.4&>0.5	24,868	4.01
	≥0.4&≤0.5	27,266	10.87
Comp_1:8	≤0.2	30,193	84
	>0.2	30,193	204

(a)

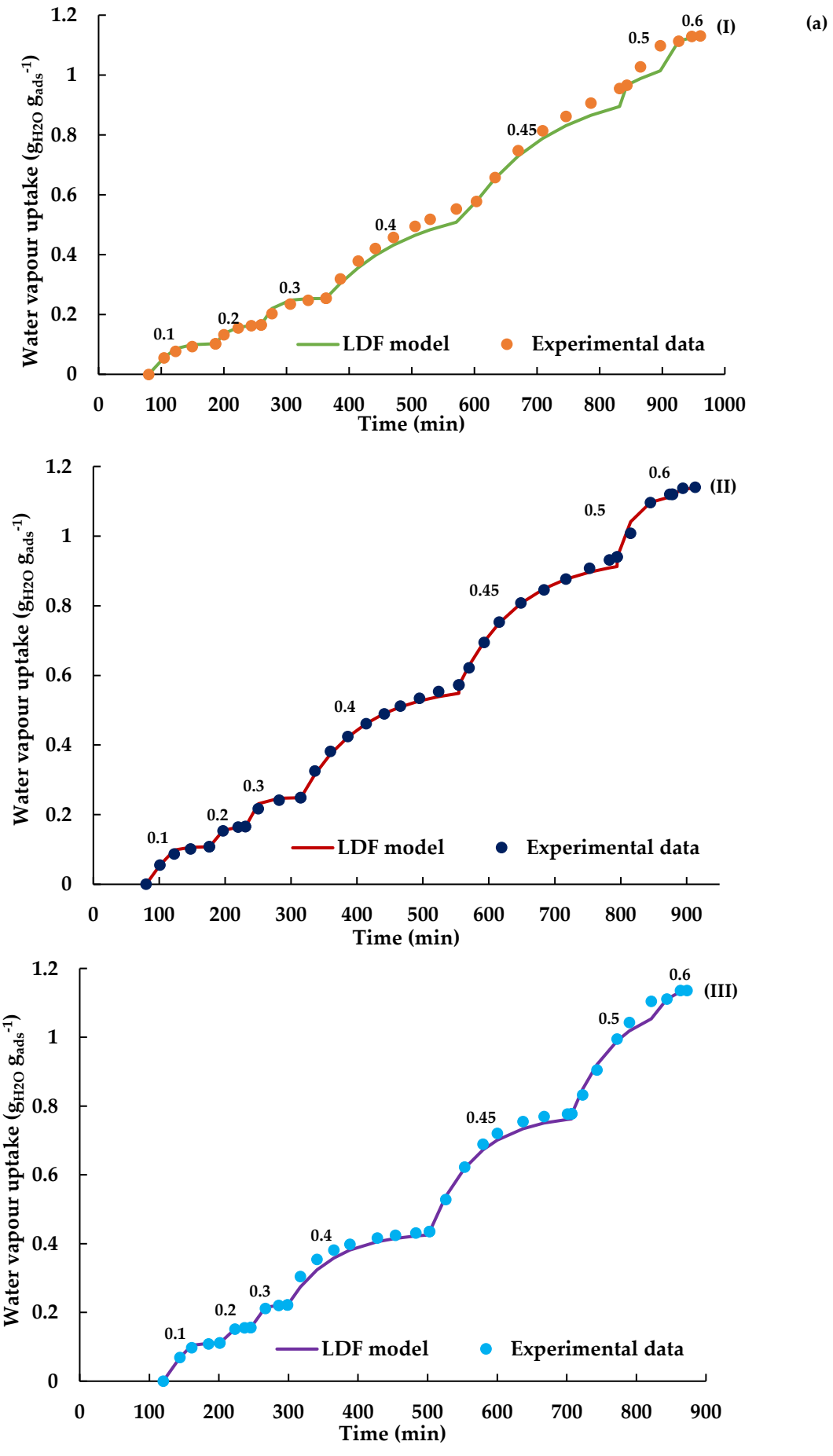
(I)
(II)
(III)
Water vapour uptake (g_{H2O} g_{ads}^{-1})
Time (min)
LDF model
Experimental data
0.1
0.2
0.3
0.4
0.45
0.5
0.6

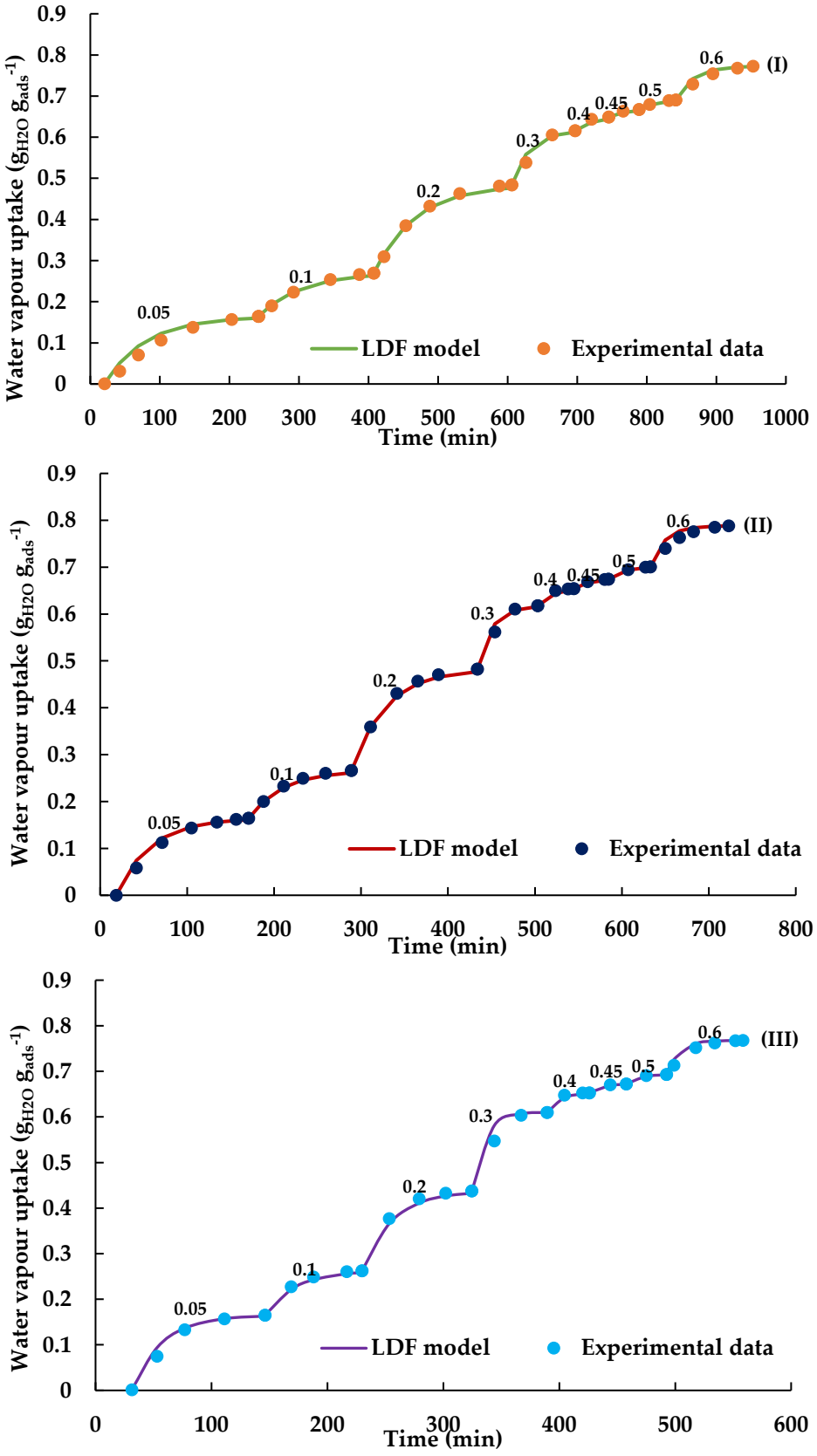

Fig. 6 a. LDF model fitting of water adsorption on Comp_1:5 at I. 15°C, II. 25°C and III. 35°C and b. LDF model fitting of water adsorption on Comp_1:8 at I. 15°C, II. 25°C and III. 35°C. (The relative pressure steps are shown above every step)

3. Ideal thermodynamic cycle of MIL-101(Cr) and $CaCl_2$ composites:

Based on the equilibrium water adsorption isotherms discussed previously, the performance of MIL-101(Cr), Comp_1:5 and Comp_1:8 composites was investigated to assess their suitability for the cooling application through assuming ideal thermodynamic cycle before the dynamic modelling of the system. Thermodynamic relation between pressure, adsorption temperature and water vapour concentration are depicted in the P-T-x diagram (**Fig. 7**). Operating conditions of typical cooling adsorption cycle were chosen. A condensation temperature and an adsorption temperature of 30°C were assumed. The regeneration temperature was 90°C and the evaporation temperature was 15°C. From the figure, it is evident that the composites surpassed the neat MIL-101(Cr). At the specified operating conditions, the Comp_1:5 $CaCl_2$ composite had a water loading difference of 0.517 $g_{H2O}\ g_{ads}^{-1}$ while the Comp_1:8 $CaCl_2$ composite had 0.53 $g_{H2O}\ g_{ads}^{-1}$ compared to only 0.093 $g_{H2O}\ g_{ads}^{-1}$ for MIL-101(Cr). Such performance motivated the authors to further investigate the performance of the three materials in a simulated real system through dynamic modelling of a two-bed system.

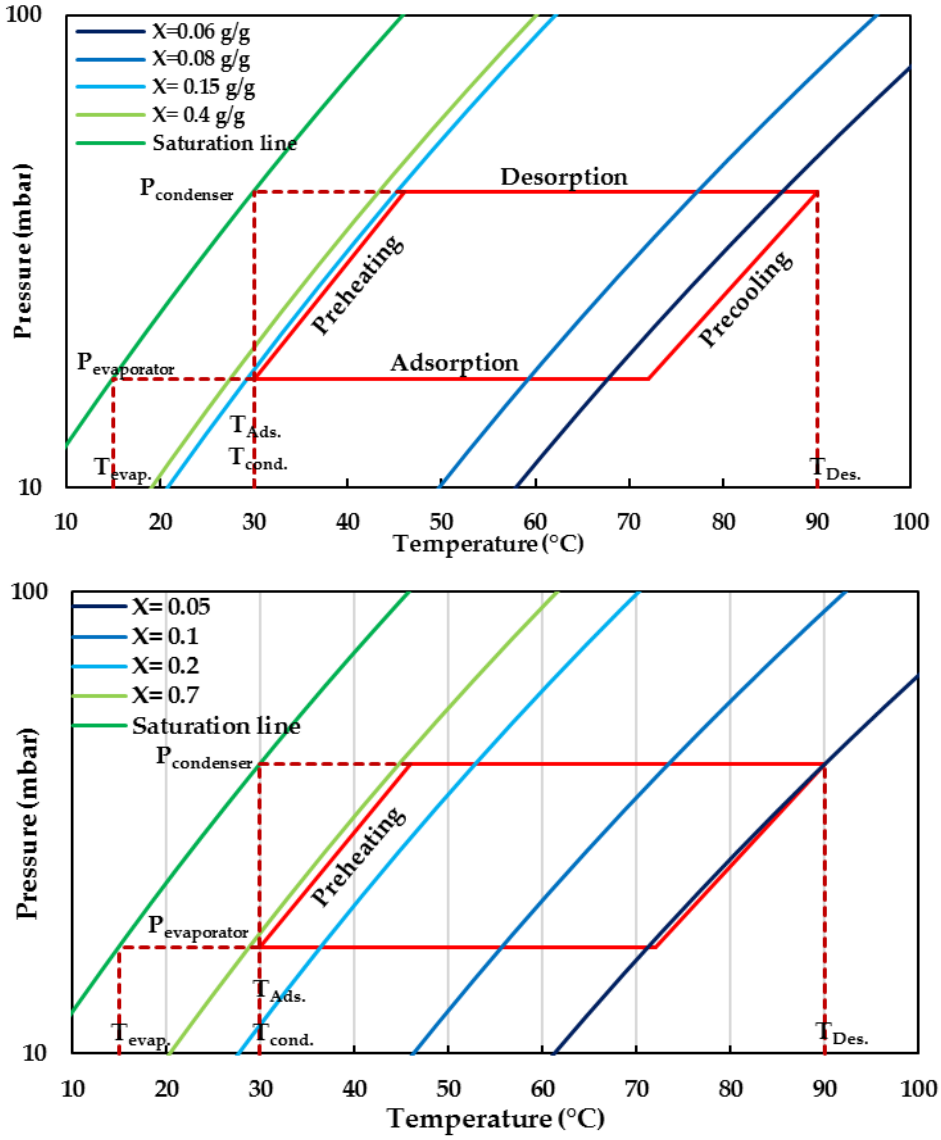

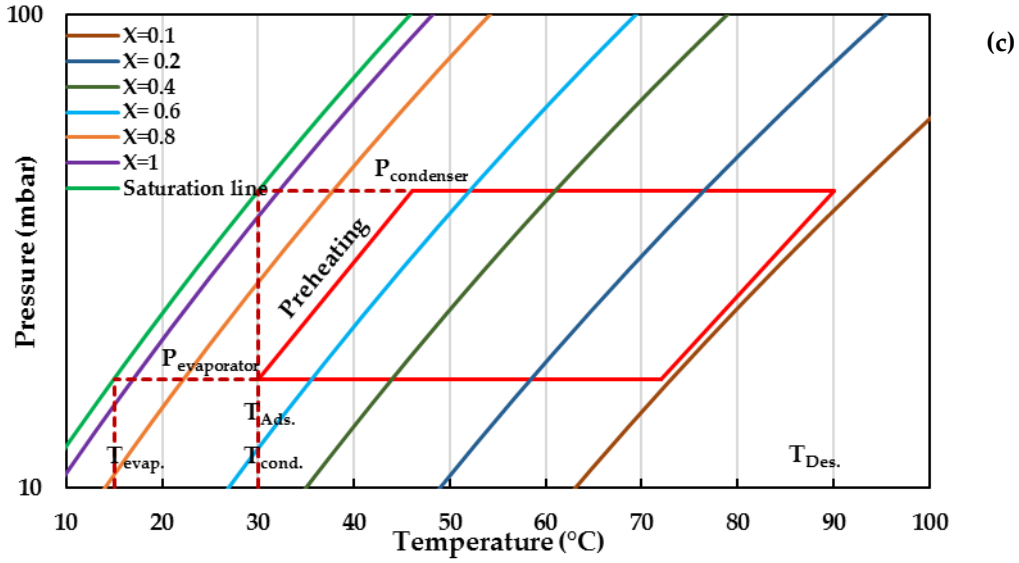

Fig. 7 P-T-x diagrams of a. MIL-101(Cr), b. Comp_1:5 and c. Comp_1:8 $CaCl_2$ composites. (Ads. Temp. = 30°C, Cond. Temp. = 30°C, Eva. Temp = 15°C and Des. Temp = 90°C).

4. Adsorption system dynamic modelling:

The adsorption system was simulated using SIMULINK to compare the performance of the synthesized composites to the neat MIL-101(Cr) and investigate the effect of chilled water inlet temperature on the performance of each material. **Fig. 8a** shows the inputs and outputs of each of the components of the system in the MATLAB/SIMULINK model while **Fig. 8b** presents the layout of SIMULINK model, showing that the system consists of an evaporator, a condenser, and two reactor adsorption heat exchangers. Signals are used to input the hot and cold fluid temperatures. Integrators are used to convert the differential signal into physical parameters values such as temperatures tracked in time. The model was built and run based on using the same dimensions and operating conditions as the adsorption cooling system mentioned in the literature (Saha et al., 1995).

The set of energy and mass balance equations shown below are solved by SIMULINK which is a lumped-parameter simulation software to simplify the governing equations. The most important assumption is that each component of the adsorption bed (tube, fins and adsorbent material) are assumed to have the same properties in every position and status during the same period of time. Therefore, the governing equations are reduced to differential equations of time, including adsorption isotherms and kinetic equations, heat transfer and mass balance equations using an ODE45 solver.

A comparative study was then held to compare the performance of the neat MIL-101(Cr) and its composites to other conventional materials such as silica gel and silica gel/$CaCl_2$ composite (SWS-1L).

The adsorption system in this study consisted of an evaporator, a condenser and two fin-tube adsorption beds (**Fig. 1**). The region between the fins is packed with the adsorbent material. The tubes are constructed from copper while the fins are made of aluminium. The evaporator is where the evaporation of water (refrigerant) takes place while, the condenser is where the desorbed water vapour is condensed. Both

components were integrated into the model as constant UA (overall rate) approach (Saha et al., 1995) with the specifications shown in **Table 3**.

(a)

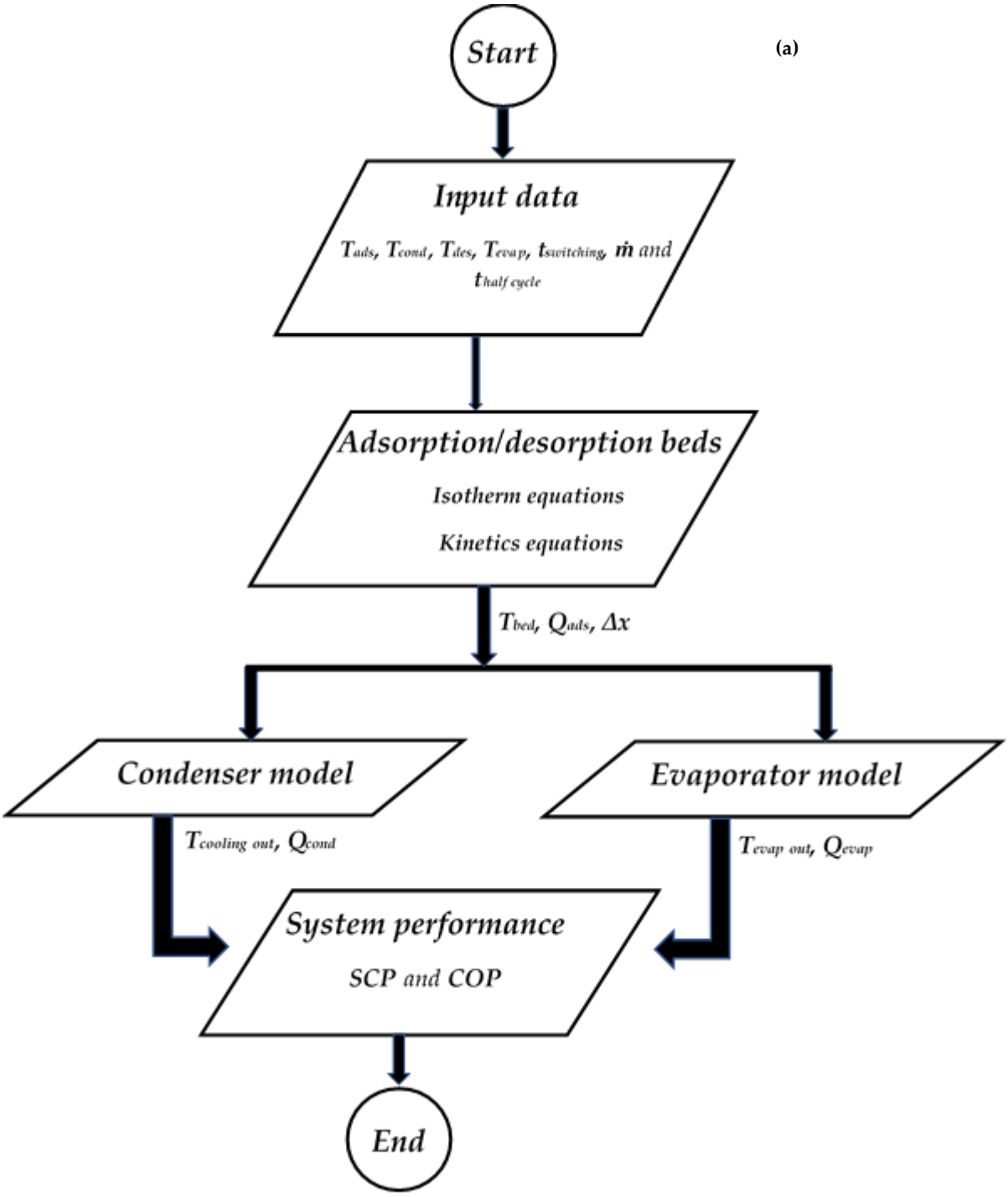

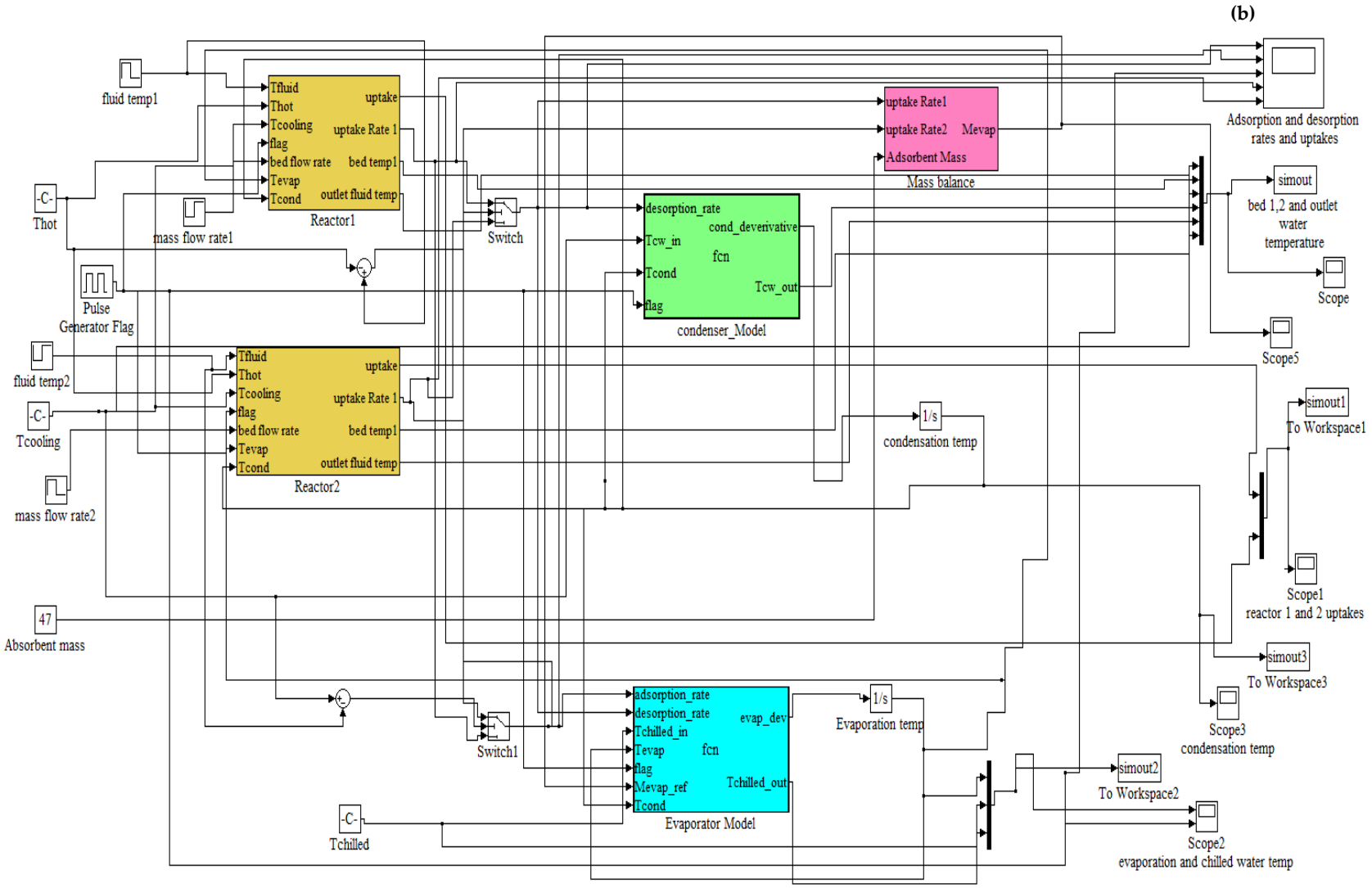

Fig. 8 a. Flowchart of the numerical model, b. two beds adsorption system SIMULINK simulation interface.

In an adsorption system, there are two main processes: heating (desorption-condensation) and cooling (adsorption-evaporation). In the adsorption phase, the bed is connected to the evaporator, cooling fluid flows through the adsorption bed so that heat of adsorption can be removed from the pre-cooled bed and the bed temperature is reduced. In the desorption phase, hot fluid flows through the bed to heat the adsorbent material and remove the adsorbed refrigerant from the adsorbent. The bed is connected to the condenser so that the spawned refrigerant is condensed. Finally, the condensate is sent back to the evaporator. Switching time is used to prepare the bed for the next adsorption or adsorption cycles. After the desorption phase, the bed pressure and temperature are high due to the residual hot fluid in the heat exchanger therefore it must be pre-cooled. While after the adsorption phase, the bed pressure and temperature are low due to the residual cold fluid in the heat exchanger therefore it must be pre-heated. During the switching processes (pre-heating/pre-cooling), all the connection valves are closed to prevent the vapour migration (Wang and Chua, 2007).

The governing equations of energy and mass balance for the adsorption/desorption beds, the evaporator and the condenser are discussed through **Eq. 12** to **Eq. 21**.

The overall mass balance recirculated in the evaporator (Elsayed et al., 2017a; Saha et al., 1995):

$$\frac{dM_{w,evap}}{dt} = -M_a \frac{dx_{des}}{dt} - M_a \frac{dx_{ads}}{dt} \tag{12}$$

The adsorption/desorption bed energy balance:

$$\left(M_a(c_{p_a} + xc_{p_{w,v}}) + M_{Cu,ads}c_{p_{Cu,ads}} + M_{Al,ads}c_{p_{Al,ads}}\right)\frac{dT_{ads}}{dt} = M_a Q_{st}\frac{dx}{dt} + \dot{m}_w c_{p_w}(T_{w,in} - T_{w,out}) \tag{13}$$

The water outlet temperature:

$$T_{w,out} = T_{ads} + \left(T_{w,in} - T_{ads}\right)\exp\left(-\frac{U_{H.Ex}SA_{H.Ex}}{\dot{m}_w c_{p_w}}\right) \tag{14}$$

The isosteric heat of adsorption:

$$Q_{st} = -R_w \frac{\partial \ln(P)}{\partial(\frac{1}{T})} \tag{15}$$

Evaporator energy balance:

$$\left(M_{w,evap}c_{p_{w,l}} + M_{cu,evap}c_{p_{cu,evap}}\right)\frac{dT_{evap}}{dt} = -\left(M_a \frac{dx_a}{dt}\right)h_{fg} - M_a c_{p_{w,l}}T_{cond}\frac{dx_{des}}{dt} + \dot{m}_{chill} c_{p_w}(T_{chill,in} - T_{chill,out}) \tag{16}$$

The chilled water outlet temperature:

$$T_{chill,out} = T_{evap} + \left(T_{chill,in} - T_{evap}\right)\exp(-\frac{U_{evap}SA_{evap}}{\dot{m}_{chill}\, c_{p_w}}) \quad \textbf{(17)}$$

The condenser energy balance:

$$\left(M_{cu,cond}c_{p_{cu,cond}}\right)\frac{dT_{cond}}{dt} = -\left(M_a\frac{dx_{des}}{dt}\right)h_{fg} + M_a c_{p_{w,l}}T_{cond}\frac{dx_{des}}{dt} + \dot{m}_{cooling}\, c_{p_w}(T_{cooling,in} - T_{cooling,out}) \quad \textbf{(18)}$$

The cooling water outlet temperature:

$$T_{cooling,out} = T_{cond} + \left(T_{cooling,in} - T_{cond}\right)\exp(-\frac{U_{cond}SA_{cond}}{\dot{m}_{cooling}\, c_{p_w}}) \quad \textbf{(19)}$$

The evaporation heat:

$$Q_{evap} = \frac{\dot{m}_{chill}\, c_{p_w}\int_0^{t_{cycle}}\left(T_{chill,in} - T_{chill,out}\right)dt}{t_{cycle}} \quad \textbf{(20)}$$

The desorption heat:

$$Q_{des} = \frac{\dot{m}_{hot}\, c_{p_w}\int_0^{t_{cycle}}\left(T_{hot,in} - T_{hot,out}\right)dt}{t_{cycle}} \quad \textbf{(21)}$$

The mathematical modelling is based on the following assumptions.

(1) The adsorbed phase and the refrigerant vapour were assumed to be liquid and gas, respectively.

(2) All adsorbent particles were uniform in size, shape and porosity, and are distributed uniformly throughout the bed.

(3) Thermal equilibrium between the adsorbed and vapour phases was assumed.

(4) The adsorption system is assumed to be perfectly insulated, which means there is no heat or mass transfer to the surroundings.

To ensure the validity and reliability of our numerical model, the results were compared with the numerical data reported by (Saha et al., 1995). The results in **Fig. 9** show the good agreement between the developed model and the previously reported numerical data. The operating conditions used in the validation are shown in **Table 3.**

To assess the performance of the system, the coefficient of performance (COP) and the specific cooling capacity (SCP) were calculated through **Eq. 22** and **Eq. 23**

The cooling coefficient of performance

$$COP_{ref} = \int_0^{t_{cycle}} \frac{Q_{evap}}{Q_{des}} dt \quad \textbf{(22)}$$

The specific cooling power:

$$SCP = \int_0^{t_{cycle}} \frac{Q_{evap}}{M_a} dt \quad \textbf{(23)}$$

The model was used to evaluate the performance of MIL-101(Cr) and its two $CaCl_2$ composites in adsorption cooling system at different chilled water inlet temperatures.

Table 3 Physical properties of silica gel and operating conditions of the system.

Term	Unit	Value
Adsorbent	Silica gel	
Number of bed	-	2
Mass of adsorbent/bed	kg	47
Mass of aluminium fins	kg	64.04
Mass of copper tubes	kg	51.2
Latent heat of adsorption	J kg^{-1}	2.8E6
Silica gel specific heat capacity	J kg^{-1} K^{-1}	924
Temp. of the heating water	°C	85
Temp. of the cooling water	°C	31
Temp. of evaporator inlet	°C	14
Temp. of condenser inlet	°C	31
Half cycle time	s	450
Switching time	s	30
Mass flow, adsorber inlet	kg s^{-1}	1.6
Mass flow, desorber inlet	kg s^{-1}	1.3
Mass flow, condenser inlet	kg s^{-1}	1.3
Mass flow, evaporator inlet	kg s^{-1}	0.7
Adsorber total heat transfer coefficient	W m^{-2} K^{-1}	1602.56
Desorber total heat transfer coefficient	W m^{-2} K^{-1}	1724.14
Condenser total heat transfer coefficient	W m^{-2} K^{-1}	4115.23
Evaporator total heat transfer coefficient	W m^{-2} K^{-1}	2557.54
Adsorber exchanging surface	m^2	2.46
Condenser exchanging surface	m^2	3.73
Evaporator exchanging surface	m^2	1.91

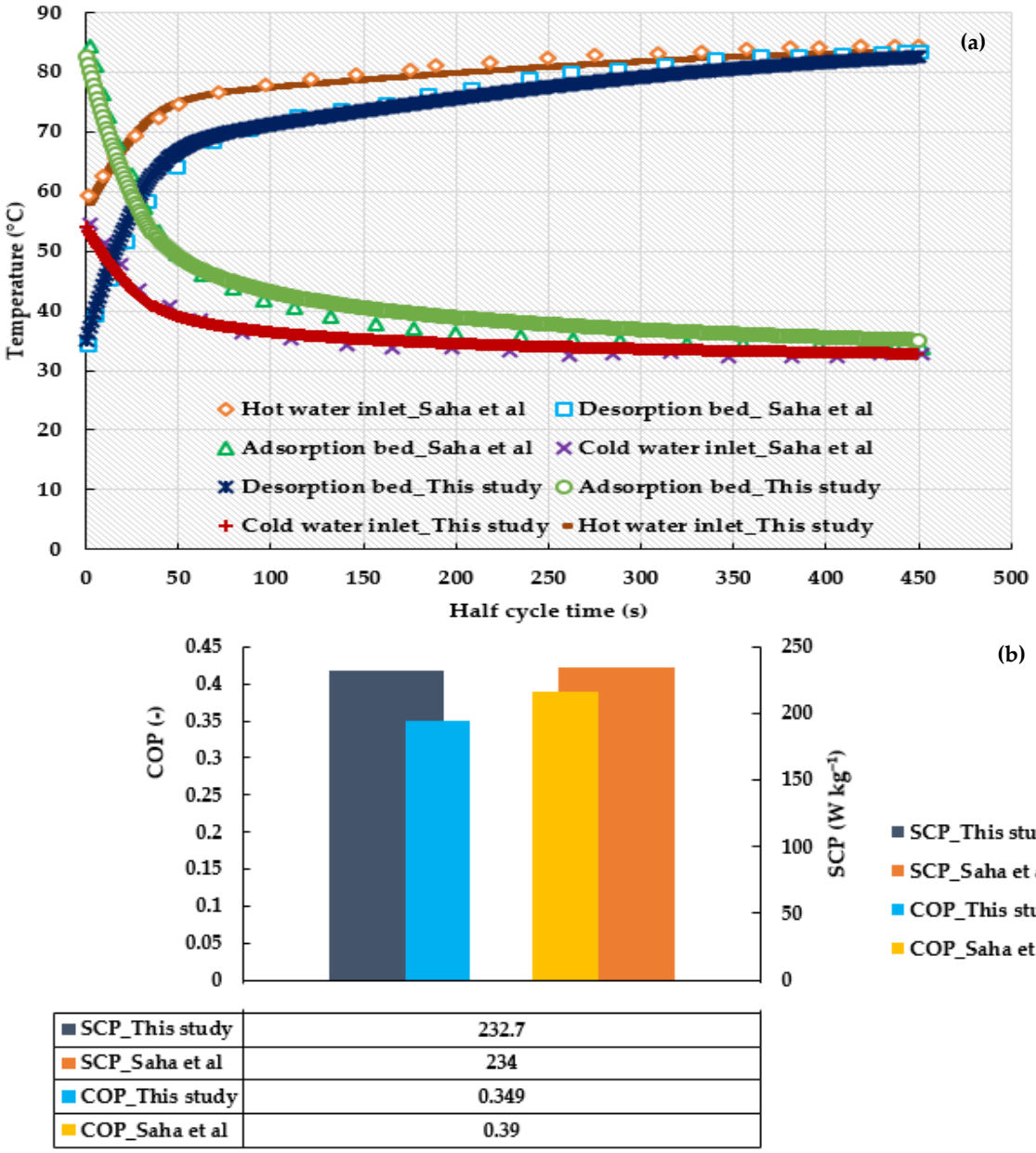

SCP_This study	232.7
SCP_Saha et al	234
COP_This study	0.349
COP_Saha et al	0.39

Fig. 9 a. Temperature profile of the developed model and reported data and b. SCP and COP of our numerical model and reported data (Saha et al., 1995).

4.1. Optimum half cycle time of MIL-101(Cr) and $CaCl_2$ composites:

Fig. 10a shows the temperature profile of the adsorption beds at the operating condition used in the P-T-x diagrams. It can be noticed that during the adsorption phase and by the end of the half cycle, Comp_1:8 had the highest temperature while MIL-101(Cr) had the lowest. This shows that the $CaCl_2$ composite requires longer half cycle time compared to the neat MIL-101(Cr) to cool down to the desired temperature. Also, during the desorption phase, MIL-101(Cr) had the highest temperature while Comp_1:8 had the lowest. Again, this shows that the $CaCl_2$ composites require longer half cycle time compared to the neat MIL-101(Cr) to heat up to the desired temperature. This temperature difference between the three materials is also an indication of the amount of adsorbed/desorbed water vapour. During the adsorption phase and as the water vapour is adsorbed, heat of adsorption is evolved hence the bed temperature is increased requiring longer adsorption time to cool down and reach the desired temperature. On the other

hand, during the desorption phase as the amount of the adsorbed water vapour increases, more heat is required to dry the material and hence longer desorption time is required. This is supported through the temperature profiles of the outlet heating and cooling fluids of the desorption and adsorption beds shown in **Fig. 10b**. It can be noticed that during the desorption phase, Comp_1:8 bed outlet had the lowest temperature while the MIL-101(Cr) had the highest. This can be attributed to that Comp_1:8 had the highest water vapour adsorbed that needs to be desorbed and hence a lower temperature of the outlet heating fluid is expected. On the other hand and during the adsorption phase, Comp_1:8 bed water outlet had the highest temperature which can be attributed to that as the water vapour is adsorbed, heat of adsorption is evolved hence the bed temperature and the outlet temperature of the cooling fluid is increased.

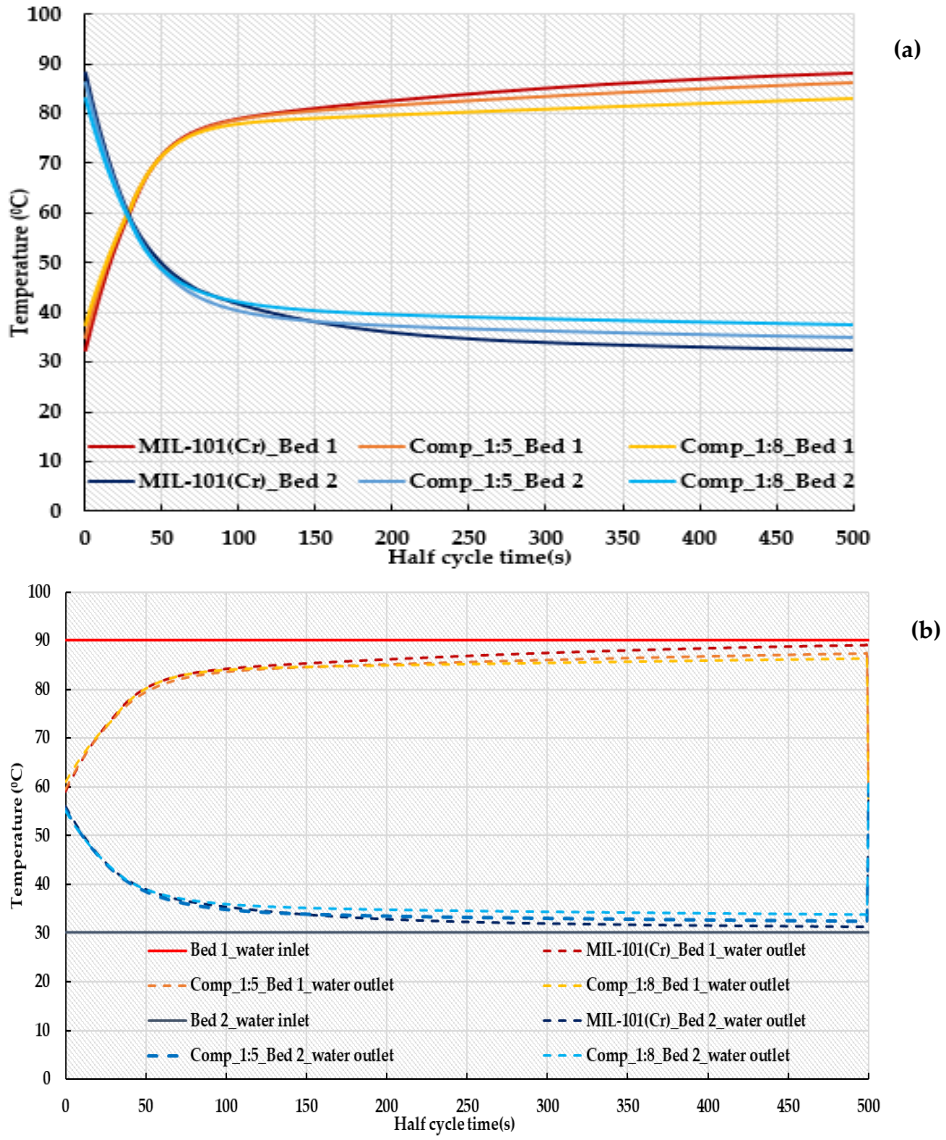

Fig. 10 a. Temperature profile of adsorption beds of MIL-101(Cr), Comp_1:5 and Comp_1:8 $CaCl_2$ composites and b. Temperature profile of inlet and outlet heating and cooling fluids of MIL-101(Cr), Comp_1:5 and Comp_1:8 $CaCl_2$ composites beds.

(Half cycle time= 500 s, switching time= 30 s, Ads. Temp. = 30°C, Cond. Temp. = 30°C, Evap. Temp = 15°C and Des. Temp = 90°C).

The optimum half cycle time of each adsorbent was investigated at different chilled water inlet temperatures. The investigated temperature range (10-17°C) was chosen according to the typical operating

conditions that can be used in adsorption cooling application. **Fig. 11a**, **Fig. 11b** and **Fig. 11c** show the optimum half cycle time of MIL-101(Cr) and the two $CaCl_2$ composites at the specified operating conditions.

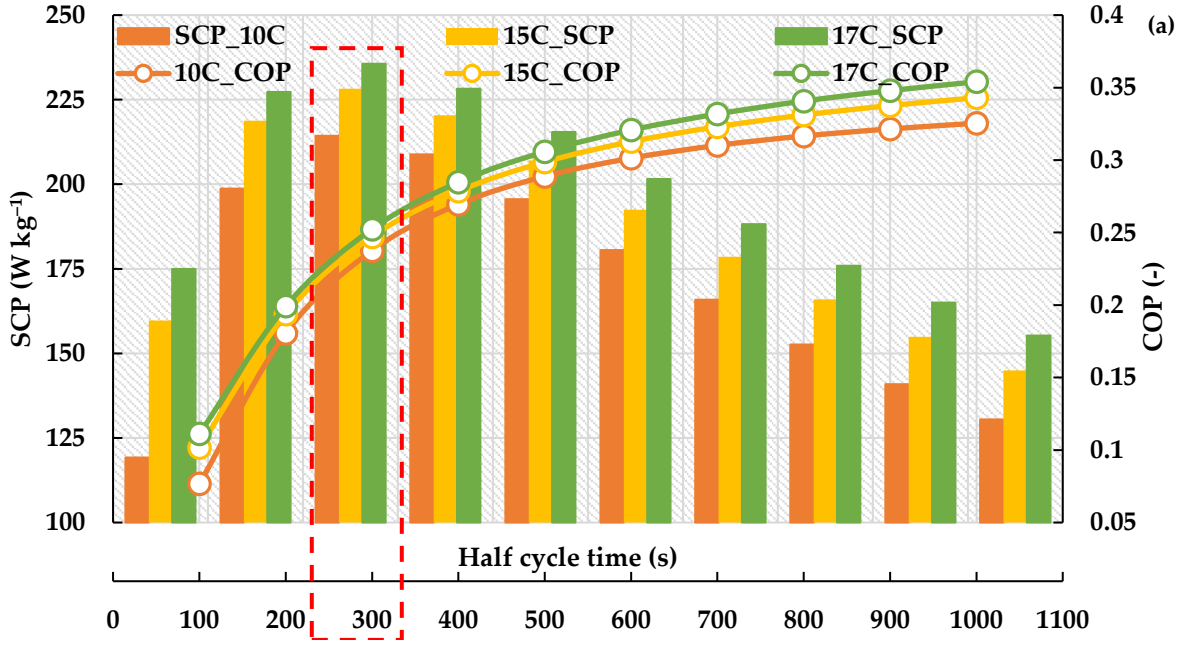

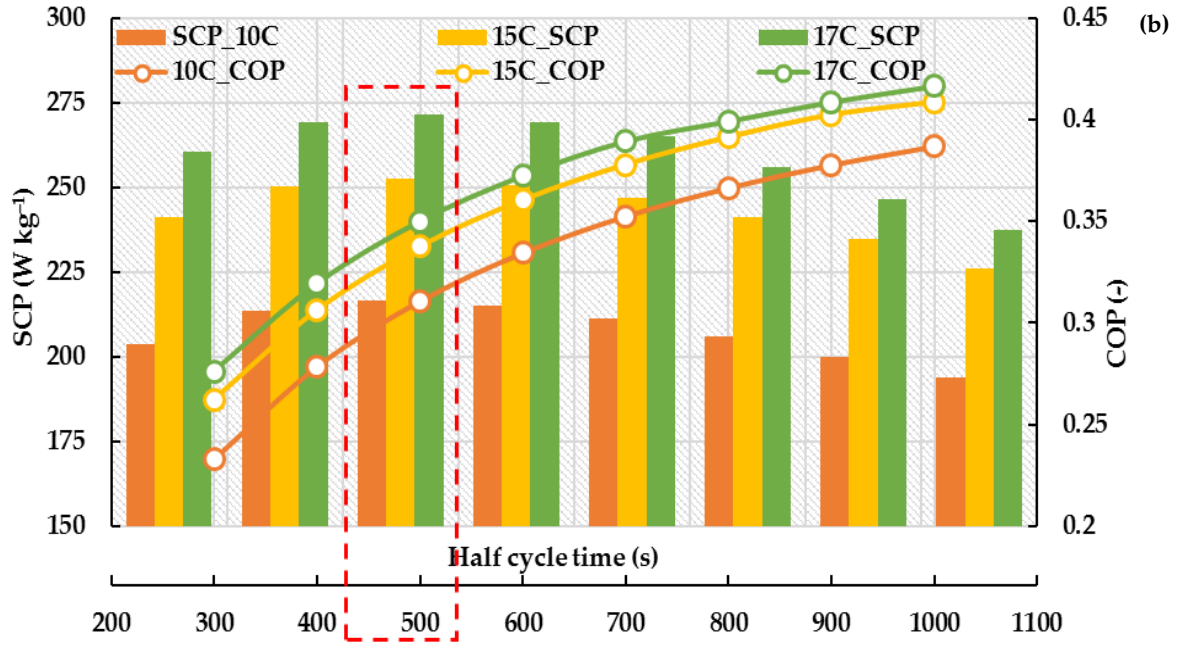

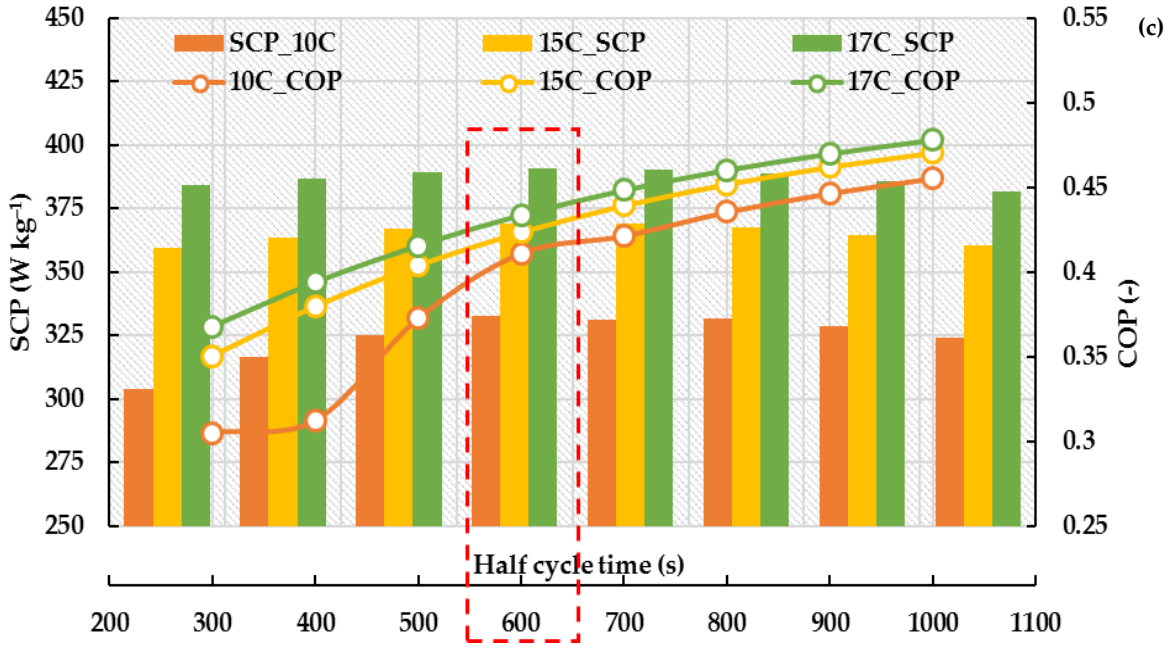

Fig. 11 Optimum half cycle time of a. MIL-101(Cr), b. Comp_1:5 and c. Comp_1:8 $CaCl_2$ composites at different chilled water inlet temperatures and a desorption temperature of 100°C.

It can be noticed that increasing the time increased the SCP of the three systems till an optimum half cycle time of 300 s in case of MIL-101(Cr), 500 s in case of the Comp_1:5 composite and 600 s in case of Comp_1:8 composite was reached. Also, it can be noticed that longer cycles were found to negatively affect the performance of the system as the SCP gradually decreased. This can be attributed to that below the optimum time, the increase in the water uptake compensates the increase in the cycle time, while as the time increases beyond the optimum cycle time, the increase in the amount of the water vapour circulated in the system is not enough to compensate the increase in time. It is also evident that at all the investigated temperatures and cycle times, the $CaCl_2$ composites outperformed the neat material based on both the SCP and COP. At a chilled water inlet temperature of 15°C and a half cycle time of 300 s, the SCP increased from 214 to 241 and 359 W kg^{-1} for the MIL-101(Cr), Comp_1:5 and Comp_1:8, respectively. This corresponds to an increase of 12% and 68% for the Comp_1:5 and Comp_1:8, respectively compared to that of MIL-101(Cr). It is evident that among the three materials, Comp_1:8 $CaCl_2$ composite had the highest performance at the different chilled water temperatures followed by Comp_1:5 $CaCl_2$ composite. Such performance is attributed to the superior water adsorption characteristics and adsorption rate of the composite.

Regarding the COP of the three systems, **Fig. 11a**, **Fig. 11b** and **Fig. 11c** show also that at all the chilled water inlet temperatures, Comp_1:8 $CaCl_2$ composite had the highest system COP followed by Comp_1:5 $CaCl_2$ composite and finally the neat MIL-101(Cr). At a chilled water inlet temperature of 15°C and a half cycle time of 500 s, the COP increased from 0.247 for MIL-101(Cr) to 0.262 and 0.35 for Comp_1:5 and Comp_1:8, respectively. **Fig. 12a**, **Fig. 12b** and **Fig. 12c** summarize the effect of the evaporation temperature on the three materials at the optimum half cycle time of 300, 500 and 600 s and at a desorption temperature of 100°C. It can be noticed that as the chilled water inlet temperature increases, both the SCP and COP increase. This can be attributed to that as the chilled water temperature increases, the working

relative pressure is increased and hence the refrigerant (water) vapour uptake and its rate increases meaning that the circulation of the adsorbate in the bed and the system performance are enhanced.

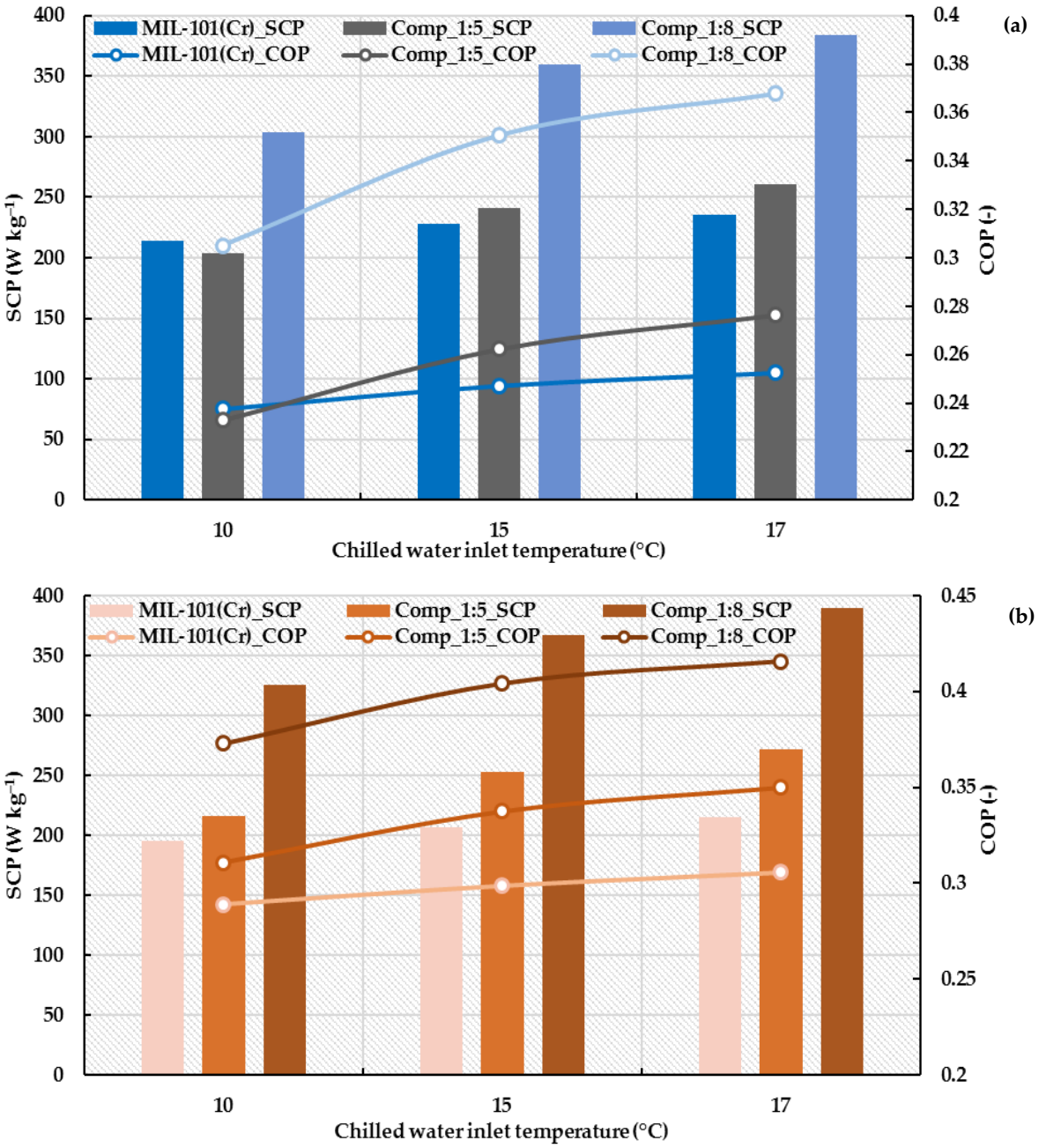

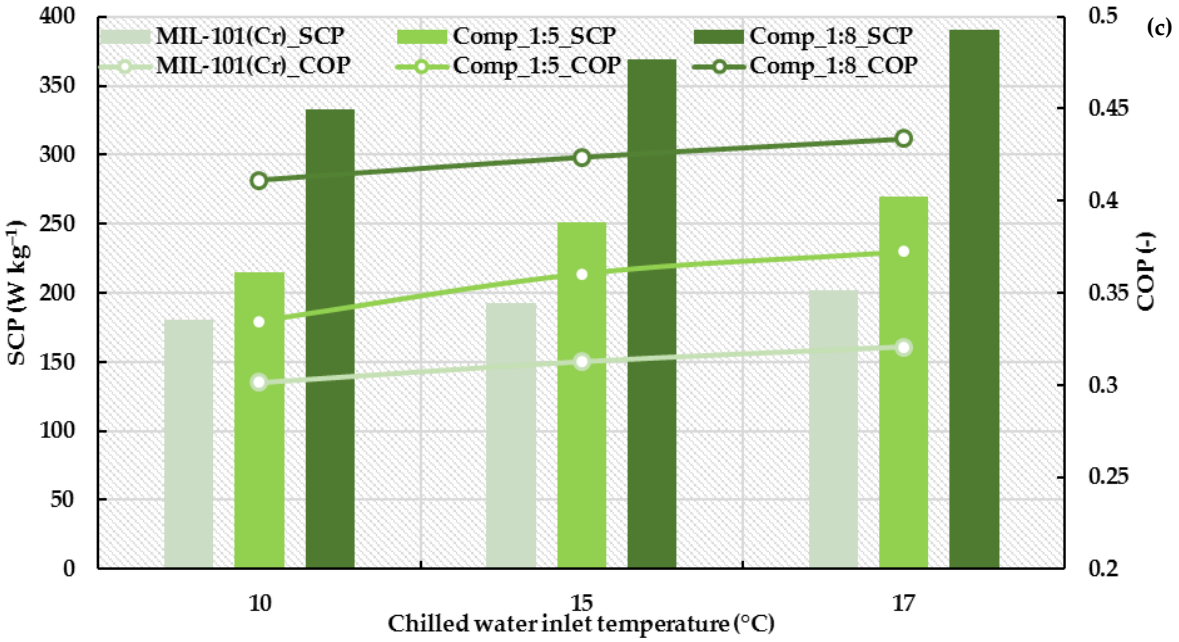

Fig. 12 Effect of chilled water inlet temperature on the SCP and COP of MIL-101(Cr), Comp_1:5 and Comp_1:8 at a half cycle time of a. 300 s, b. 500 s and c. 600 s and a desorption temperature of 100°C

4.2. Optimum desorption temperature of MIL-101(Cr) and $CaCl_2$ composites:

Fig. 13a, Fig. 13b and **Fig. 13c** show the effect of the desorption temperature on the performance of the neat MIL-101(Cr) and its $CaCl_2$ composites. It can be observed that the optimum desorption temperature of the MIL-101(Cr) is 110°C while it was found to be 90°C for the $CaCl_2$ composites. The low COP below this temperature is because the heating fluid inlet temperature is insufficient for the desorption process. At temperatures higher than the optimum desorption temperature, the COP decreases once again as the heat source temperature provides higher sensible heat for the fixed amount of refrigerant per adsorption cycle. The $CaCl_2$ composites had a lower desorption temperature of 90°C. This shows that incorporating the MIL-101(Cr) with $CaCl_2$ not only improved the water adsorption uptake but also improved the mass transfer rate and decreased the desorption temperature required to dry the material.

This lower desorption temperature means that the composites are suitable for adsorption cooling applications driven by low temperature heat sources such as waste heat or solar energy. As the systems based on composites can be driven by a lower desorption temperature, the energy required for the desorption process is reduced and hence the COP of the systems is increased.

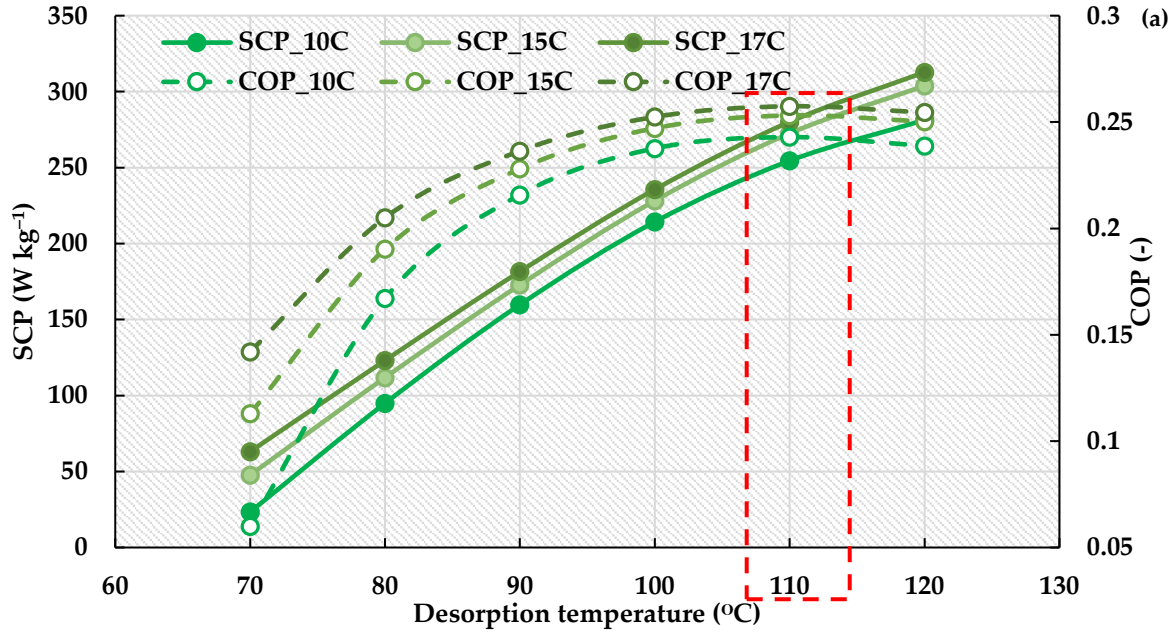
(a)
SCP_10C
SCP_15C
SCP_17C
COP_10C
COP_15C
COP_17C
SCP (W kg⁻¹)
COP (-)
Desorption temperature (°C)
350
300
250
200
150
100
50
0
0.3
0.25
0.2
0.15
0.1
0.05
60
70
80
90
100
110
120
130

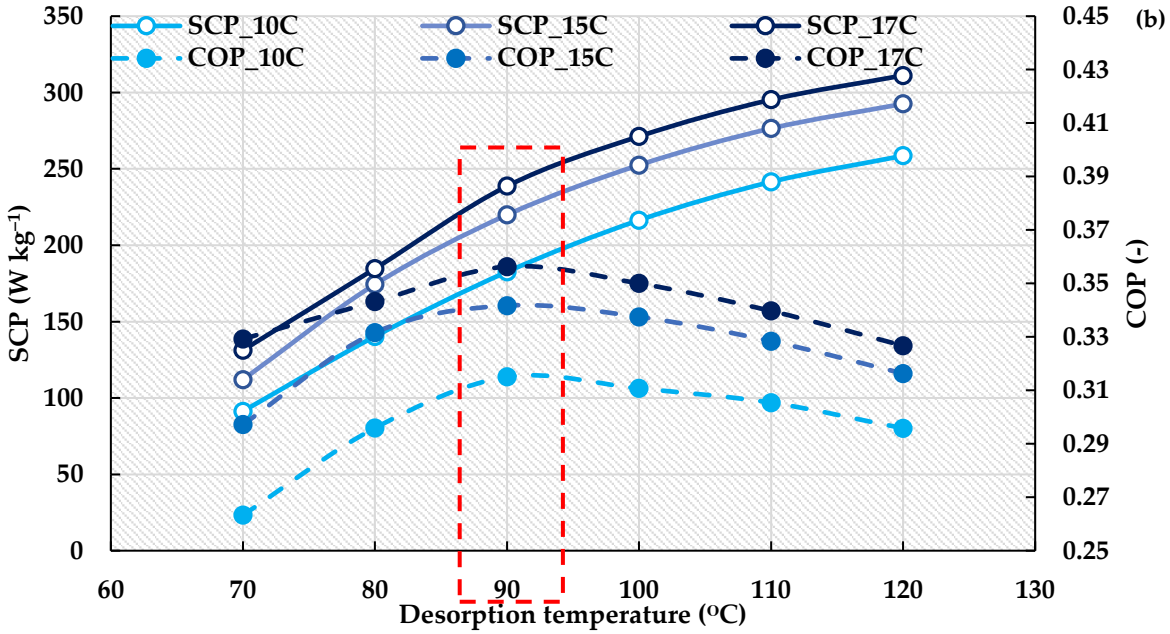
(b)
SCP_10C
SCP_15C
SCP_17C
COP_10C
COP_15C
COP_17C
SCP (W kg⁻¹)
COP (-)
Desorption temperature (°C)
350
300
250
200
150
100
50
0
0.45
0.43
0.41
0.39
0.37
0.35
0.33
0.31
0.29
0.27
0.25
60
70
80
90
100
110
120
130

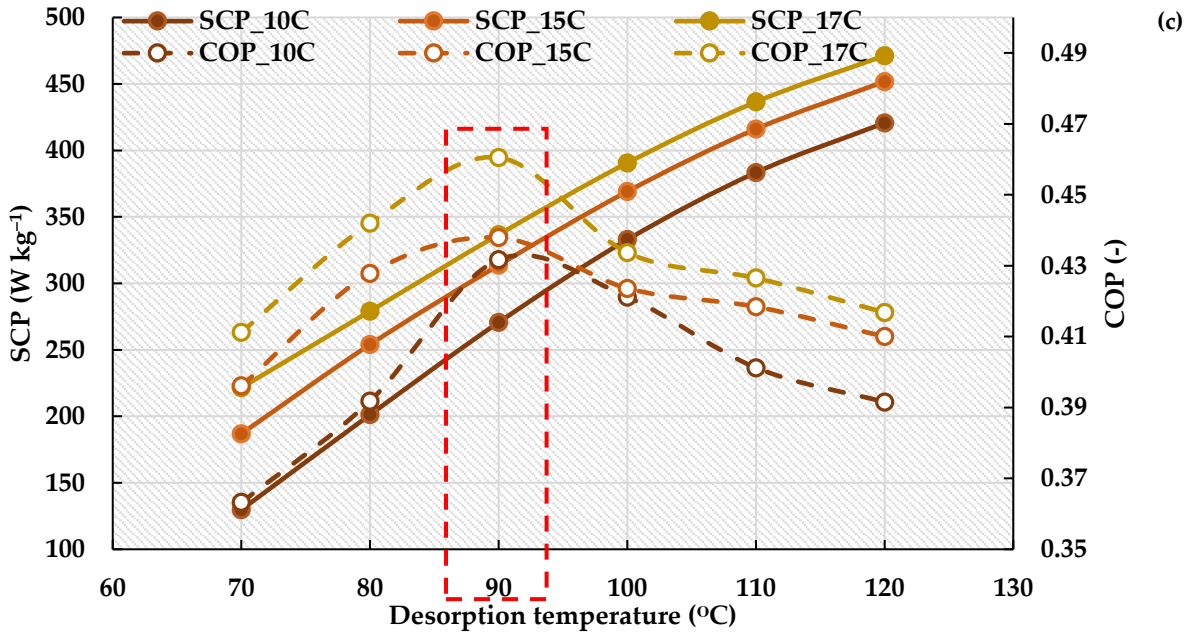

Fig. 13 Optimum desorption temperature of a. MIL-101(Cr), b. Comp_1:5 and c. Comp_1:8 $CaCl_2$ composites at different chilled water inlet temperatures.

4.3. MIL-101(Cr)/$CaCl_2$ composites: A comparative study

The performance of MIL-101(Cr) and its $CaCl_2$ composites was compared to that of the conventional and widely used silica gel and its $CaCl_2$ composite, SWS-1L. The comparison was held at different chilled water inlet temperatures, an adsorption and condensation temperature of 30°C, a half cycle time of 500 s and a desorption temperature of 90°C. The comparison was based on using adsorbent constant mass and constant volume basis. The physical properties of silica gel and SWS-1L can be found in (Saha et al., 1995; Saha et al., 2009).

Fig. 14a and **Fig. 14b** illustrate the SCP and COP values at the specified operating conditions. It can be noticed that the $CaCl_2$ significantly enhanced the performance as the two composites exhibited an improved performance compared to the neat MIL-101(Cr).

At the constant mass basis, it can be noticed that silica gel outperformed MIL-101(Cr) and Comp_1:5 at all the investigated temperatures while the Comp_1:8 outperformed silica gel. Nevertheless, SWS-1L outperformed Comp_1:8.

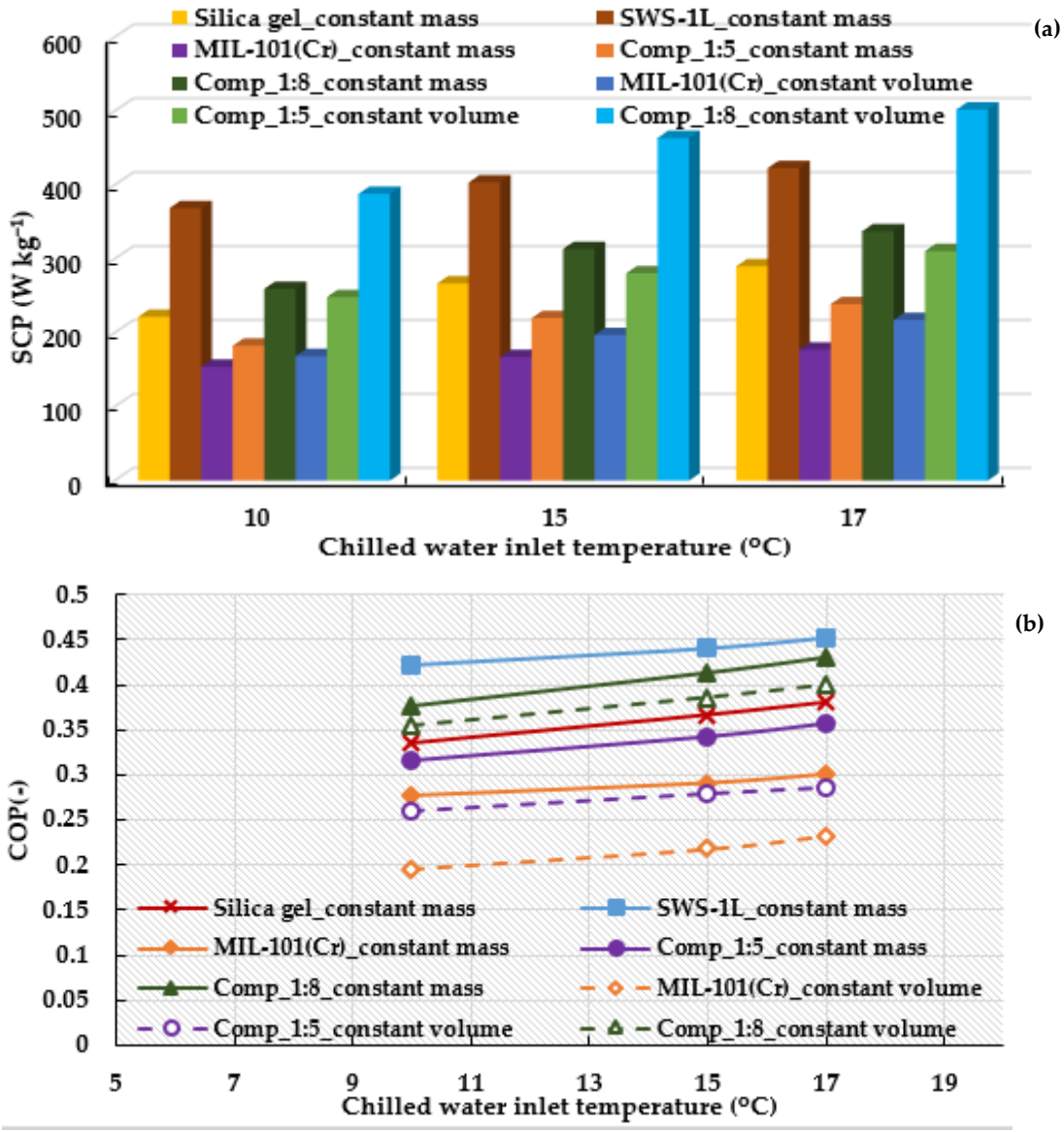

Fig. 14 Comparison of a. SCP and b. COP of silica gel, MIL-101(Cr) and $CaCl_2$ composites at a desorption temperature of 90°C and 500 s.

Regarding the COP of the systems, MIL-101(Cr) had the lowest COP while Comp_1:8 had a slightly lower COP compared to SWS-1L. The improved composite performance can be attributed to that the amount of water vapour circulated for each material at the investigated operating conditions as the MIL-101(Cr) had the lowest while Comp_1:8 had much higher amount.

In adsorption systems, the adsorbent materials are packed based on a constant volume basis. In this case and due to the low MOF density (Usman et al., 2017; Zhang et al., 2017), a lower amount of adsorbent is used compared to silica gel and SWS-1L. The packing density of Comp_1:5 and Comp_1:8 were 319 and 373 kg m^{-3}, respectively. Also, as the amount of adsorbent is decreased, the heat and mass transfer processes are expected to be significantly enhanced. This causes the SCP to increase as it is inversely proportional to the mass of the adsorbent. In this case, it can be noticed that the Comp_1:5 outperformed MIL-101(Cr) and silica gel while Comp_1:8 produced the highest SCP among all the materials under investigation

including SWS-1L at all the investigated temperatures producing a significantly higher cooling effect compared to silica gel and SWS-1L.

On the other hand, it can be noticed that decreasing the adsorbent mass decreased the COP of the system. The lower COP of the MIL-101(Cr) and its $CaCl_2$ composites systems compared to the silica gel system may be attributed to the low adsorbent mass to metal mass ratio due to the low density of the MOF materials (Aristov et al., 2012; Rezk et al., 2012). This comparative study highlights the potential of a new generation of adsorbent materials composites with its improved adsorption capacity and kinetics which can result in a more energy efficient and compact systems.

5. Conclusions

MIL-101(Cr) has exceptionally high-water adsorption uptake of around 1.47 g_{H2O} g_{ads}^{-1} due to its high surface area and pore volume. Nevertheless, such superior performance is only obtained at high relative pressure (>0.5) which makes it impractical as an adsorbent for adsorption cooling application. Novel composites of MIL-101(Cr)/$CaCl_2$ were synthesized, showing enhanced water vapour uptake in the low-relative pressure range. Therefore, this work investigates the potential of MIL-101(Cr)/$CaCl_2$ composites in adsorption cooling application. The synthesized composites showed a half cycle time of 500 and 600 s with a superior SCP and COP values compared to the parent MIL-101(Cr). Also, introducing the $CaCl_2$ to the MIL-101(Cr) decreased the desorption temperature from 110°C to 90°C. The effect of the chilled water inlet temperature was investigated for the three materials, showing that increasing the chilled water inlet temperature increased the SCP and the COP.

A comparative study was held comparing the performance of the synthesized composites to silica gel and SWS-1L at constant volume and constant mass basis. It was found that the composites specially Comp_1:8 outperformed silica gel and SWS-1L giving the highest SCP on the constant volume basis.

This work proves that introducing $CaCl_2$ to MIL-101(Cr) enhanced the water vapour uptake and significantly enhanced the performance of the system paving the way for using a new generation of more efficient adsorbent materials.

Uncategorized References

Ali, E.S., Askalany, A.A., Harby, K., Diab, M.R., Alsaman, A.S., 2018. Adsorption desalination-cooling system employing copper sulfate driven by low grade heat sources. Applied Thermal Engineering 136, 169-176.

Aristov, Y.I., Glaznev, I.S., Girnik, I.S., 2012. Optimization of adsorption dynamics in adsorptive chillers: loose grains configuration. Energy 46, 484-492.

Aristov, Y.I., Restuccia, G., Cacciola, G., Parmon, V., 2002. A family of new working materials for solid sorption air conditioning systems. Applied Thermal Engineering 22, 191-204.

Aristov, Y.I., Tokarev, M., Cacciola, G., Restuccia, G., 1996. Selective water sorbents for multiple applications, 1. CaCl 2 confined in mesopores of silica gel: sorption properties. Reaction Kinetics and Catalysis Letters 59, 325-333.

Bimbo, N., Xu, W., Sharpe, J.E., Ting, V.P., Mays, T.J., 2016. High-pressure adsorptive storage of hydrogen in MIL-101 (Cr) and AX-21 for mobile applications: cryocharging and cryokinetics. Materials & Design 89, 1086-1094.

Chan, K.C., Chao, C.Y., Sze-To, G., Hui, K.S., 2012. Performance predictions for a new zeolite 13X/CaCl2 composite adsorbent for adsorption cooling systems. International Journal of Heat and Mass Transfer 55, 3214-3224.

Critoph, R.E., Metcalf, S.J., Tamainot-Telto, Z., 2010. Proof of concept car adsorption air-conditioning system using a compact sorption reactor. Heat Transfer Engineering 31, 950-956.
Ehrenmann, J., Henninger, S.K., Janiak, C., 2011. Water Adsorption Characteristics of MIL-101 for Heat-Transformation Applications of MOFs. European Journal of Inorganic Chemistry 2011, 471-474.
El-Sharkawy, I.I., Uddin, K., Miyazaki, T., Saha, B.B., Koyama, S., Kil, H.-S., Yoon, S.-H., Miyawaki, J., 2015. Adsorption of ethanol onto phenol resin based adsorbents for developing next generation cooling systems. International Journal of Heat and Mass Transfer 81, 171-178.
El-Sharkawy, I.I., Uddin, K., Miyazaki, T., Saha, B.B., Koyama, S., Miyawaki, J., Yoon, S.-H., 2014. Adsorption of ethanol onto parent and surface treated activated carbon powders. International Journal of Heat and Mass Transfer 73, 445-455.
Elsayed, A., Elsayed, E., Raya, A.-D., Mahmoud, S., Elshaer, A., Kaialy, W., 2017a. Thermal energy storage using metal–organic framework materials. Applied Energy 186, 509-519.
Elsayed, E., Anderson, P., Raya, A.-D., Mahmoud, S., Elsayed, A.J.J.o.S.S.C., 2019. MIL-101 (Cr)/calcium chloride composites for enhanced adsorption cooling and water desalination.
Elsayed, E., Wang, H., Anderson, P.A., Al-Dadah, R., Mahmoud, S., Navarro, H., Ding, Y., Bowen, J., 2017b. Development of MIL-101 (Cr)/GrO composites for adsorption heat pump applications. Microporous and Mesoporous Materials 244, 180-191.
Férey, G., Mellot-Draznieks, C., Serre, C., Millange, F., Dutour, J., Surblé, S., Margiolaki, I.J.S., 2005. A chromium terephthalate-based solid with unusually large pore volumes and surface area. 309, 2040-2042.
Goldmann, F., Polanyi, M., 1928. Adsorption von Dämpfen an Kohle und die Wärmeausdehnung der Benutzungsschicht. Zeitschrift für Physikalische Chemie 132, 321-370.
Graf, S., Lanzerath, F., Sapienza, A., Frazzica, A., Freni, A., Bardow, A., 2016. Prediction of scp and cop for adsorption heat pumps and chillers by combining the large-temperature-jump method and dynamic modeling. Applied Thermal Engineering 98, 900-909.
Hamamoto, Y., Alam, K.A., Akisawa, A., Kashiwagi, T., 2005. Performance evaluation of a two-stage adsorption refrigeration cycle with different mass ratio. International journal of refrigeration 28, 344-352.
Henley, J., 2015. World set to use more energy for cooling than heating. The Guardian 26.
Henninger, S.K., Habib, H.A., Janiak, C., 2009. MOFs as adsorbents for low temperature heating and cooling applications. Journal of the American Chemical Society 131, 2776-2777.
Henninger, S.K., Jeremias, F., Kummer, H., Janiak, C., 2012. MOFs for use in adsorption heat pump processes. European Journal of Inorganic Chemistry 2012, 2625-2634.
Janiak, C., Henninger, S.K., 2013. Porous coordination polymers as novel sorption materials for heat transformation processes. CHIMIA International Journal for Chemistry 67, 419-424.
Jeremias, F., Fröhlich, D., Janiak, C., Henninger, S.K., 2014. Advancement of sorption-based heat transformation by a metal coating of highly-stable, hydrophilic aluminium fumarate MOF. RSC Advances 4, 24073-24082.
Jeremias, F., Khutia, A., Henninger, S.K., Janiak, C., 2012. MIL-100 (Al, Fe) as water adsorbents for heat transformation purposes—a promising application. Journal of Materials Chemistry 22, 10148-10151.
Khan, M., Alam, K., Saha, B., Hamamoto, Y., Akisawa, A., Kashiwagi, T., 2006. Parametric study of a two-stage adsorption chiller using re-heat—The effect of overall thermal conductance and adsorbent mass on system performance. International journal of thermal sciences 45, 511-519.
Khutia, A., Rammelberg, H.U., Schmidt, T., Henninger, S., Janiak, C., 2013. Water sorption cycle measurements on functionalized MIL-101Cr for heat transformation application. Chemistry of Materials 25, 790-798.
Lefebvre, D., Amyot, P., Ugur, B., Tezel, F.H., 2016. Adsorption Prediction and Modeling of Thermal Energy Storage Systems: A Parametric Study. Industrial & Engineering Chemistry Research 55, 4760-4772.
Mande, S., Ghosh, P., Kishore, V., Oertel, K., Sprengel, U., 2000. Development of an advanced solar–hybrid adsorption cooling system for decentralized storage of agricultural products in India. Tata Energy Research Institute. India., Deutsche Forschungsanstalt für Luft-und Raumfahrt eV Germany.
Narayanan, S., Yang, S., Kim, H., Wang, E.N., 2014. Optimization of adsorption processes for climate control and thermal energy storage. International Journal of Heat and Mass Transfer 77, 288-300.

Niazmand, H., Talebian, H., Mahdavikhah, M., 2013. Effects of particle diameter on performance improvement of adsorption systems. Applied Thermal Engineering 59, 243-252.
Polanyi, M., 1963. The potential theory of adsorption. Science 141, 1010-1013.
Poyelle, F., Guilleminot, J.-J., Meunier, F., 1999. Experimental tests and predictive model of an adsorptive air conditioning unit. Industrial & engineering chemistry research 38, 298-309.
Qadir, N.U., Said, S.A., Mansour, R.B., Mezghani, K., Ul-Hamid, A., 2016. Synthesis, characterization, and water adsorption properties of a novel multi-walled carbon nanotube/MIL-100 (Fe) composite. Dalton Transactions 45, 15621-15633.
Rezk, A., Al-Dadah, R., Mahmoud, S., Elsayed, A., 2012. Characterisation of metal organic frameworks for adsorption cooling. International journal of heat and mass transfer 55, 7366-7374.
Rezk, A., Al-Dadah, R., Mahmoud, S., Elsayed, A., 2013. Experimental investigation of metal organic frameworks characteristics for water adsorption chillers. Proceedings of the Institution of Mechanical Engineers, Part C: Journal of Mechanical Engineering Science 227, 992-1005.
Rouquerol, J., Rouquerol, F., Llewellyn, P., Maurin, G., Sing, K.S., 2013. Adsorption by powders and porous solids: principles, methodology and applications. Academic press.
Saha, B.B., Boelman, E.C., Kashiwagi, T., 1995. Computer simulation of a silica gel-water adsorption refrigeration cycle-the influence of operating conditions on cooling output and COP. ASHRAE transactions: research 101, 348-357.
Saha, B.B., Chakraborty, A., Koyama, S., Aristov, Y.I.J.I.J.o.H., Transfer, M., 2009. A new generation cooling device employing CaCl2-in-silica gel–water system. 52, 516-524.
Saha, B.B., Chakraborty, A., Ng, K.C., 2011. Innovative Materials for Processes in Energy Systems-For Fuel Cells, Heat Pumps and Sorption Systems. Research Publishing Service.
Saha, P., Chowdhury, S., 2011. Insight into adsorption thermodynamics, Thermodynamics. InTech.
Schicktanz, M., Núñez, T., 2009. Modelling of an adsorption chiller for dynamic system simulation. International Journal of Refrigeration 32, 588-595.
Sultan, M., El-Sharkawy, I.I., Miyazaki, T., Saha, B.B., Koyama, S., Maruyama, T., Maeda, S., Nakamura, T., 2016. Water vapor sorption kinetics of polymer based sorbents: Theory and experiments. Applied Thermal Engineering 106, 192-202.
Tokarev, M., Okunev, B., Safonov, M., Kheifets, L., Aristov, Y.I., 2005. Approximation Equations for Describing the Sorption Equilibrium between Water Vapor and a CaCl~ 2-in-Silica Gel Composite Sorbent. RUSSIAN JOURNAL OF PHYSICAL CHEMISTRY C/C OF ZHURNAL FIZICHESKOI KHIMII 79, 1490.
Tso, C.Y., Chao, C.Y., 2012. Activated carbon, silica-gel and calcium chloride composite adsorbents for energy efficient solar adsorption cooling and dehumidification systems. International Journal of Refrigeration 35, 1626-1638.
Usman, M., Mendiratta, S., Lu, K.L., 2017. Semiconductor Metal–Organic Frameworks: Future Low-Bandgap Materials. Advanced Materials 29, 1605071.
Wang, J., Wang, R., Wang, L., 2016. Water vapor sorption performance of ACF-CaCl 2 and silica gel-CaCl 2 composite adsorbents. Applied Thermal Engineering 100, 893-901.
Wang, X., Chua, H., 2007. Two bed silica gel–water adsorption chillers: an effectual lumped parameter model. International Journal of Refrigeration 30, 1417-1426.
Wu, J., Wang, R., Xu, Y., 2002. Dynamic analysis of heat recovery process for a continuous heat recovery adsorption heat pump. Energy conversion and management 43, 2201-2211.
Yan, J., Yu, Y., Ma, C., Xiao, J., Xia, Q., Li, Y., Li, Z., 2015. Adsorption isotherms and kinetics of water vapor on novel adsorbents MIL-101 (Cr)@ GO with super-high capacity. Applied thermal engineering 84, 118-125.
Yang, J., Zhao, Q., Li, J., Dong, J., 2010. Synthesis of metal–organic framework MIL-101 in TMAOH-Cr (NO 3) 3-H 2 BDC-H 2 O and its hydrogen-storage behavior. Microporous and Mesoporous Materials 130, 174-179.
Zhang, H., Nai, J., Yu, L., Lou, X.W.D., 2017. Metal-organic-framework-based materials as platforms for renewable energy and environmental applications. Joule 1, 77-107.
Zhang, X., Dincer, I., 2017. Energy Solutions to Combat Global Warming. Springer.
Zhao, T., Jeremias, F., Boldog, I., Nguyen, B., Henninger, S.K., Janiak, C.J.D.T., 2015. High-yield, fluoride-free and large-scale synthesis of MIL-101 (Cr). 44, 16791-16801.

Zhengqiu, R., Quanguo, L., Qun, C., Haiyan, W., Haijun, C., Huqing, Y., 2014. Adsorption refrigeration performance of shaped MIL-101-water working pair. Chinese Journal of Chemical Engineering 22, 570-575.